DTU Library

Kinetics and Mechanisms of Oxygen Surface Exchange on La0.6Sr0.4FeO3-delta Thin Films

Mosleh, Majid; Søgaard, Martin; Hendriksen, Peter Vang

Link back to DTU Orbit

Kinetics and Mechanisms of Oxygen Surface Exchange on La$_{0.6}$Sr$_{0.4}$FeO$_{3-\delta}$ Thin Films

Majid Mosleh, Martin Søgaard, and Peter Vang Hendriksen[z]

Department of Fuel Cells and Solid State Chemistry, Risø National Laboratory for Sustainable Energy, Technical University of Denmark, DK-4000 Roskilde, Denmark

The thermodynamic properties as well as oxygen exchange kinetics were examined on mixed ionic and electronic conducting (La$_{0.6}$Sr$_{0.4}$)$_{0.99}$FeO3$_{-\delta}$ (LSF64) thin films deposited on MgO single crystals. It is found that thin films and bulk material have the same oxygen stoichiometry for a given temperature and oxygen partial pressure [i.e., the incorporation reaction has the same reaction enthalpy ($\Delta H^0 = -105$ KJ/mol) and entropy ($\Delta S^0 = -75.5$ J/mol/K) as found for bulk material]. The thin film shows smaller apparent electrical conductivity than reported for bulk. This is due to imperfections in the film, which is not totally dense and contains closed porosity. Electrical conductivity relaxation was used to determine the surface exchange coefficient and its dependence on the temperature and oxygen partial pressure. Relaxation curves showed a good fit to a simple exponential decay. The vacancy surface exchange coefficient (k_V) determined from K_{chem} shows a slope (log k_V vs log P_{O_2}) between 0.51 and 0.85. It is further found that k_V is proportional to the product of the oxygen partial pressure and the vacancy concentration ($k_V \propto P_{O_2}\delta_\infty$). Different reaction mechanisms that can account for the observed P_{O_2} and δ-dependence of k_V are analyzed. It is proposed that the vacancies are the active sites of adsorption of molecular oxygen and that the rate determining step for the exchange reaction is splitting of the adsorbed oxygen.

© 2009 The Electrochemical Society. [DOI: 10.1149/1.3062941] All rights reserved.

Mixed ionic and electronic conductors (MIECs) have potential applications in solid oxide fuel cells (SOFCs), oxygen separation membranes, and thin-film sensors. One group of promising materials with high oxygen-ion conductivity, good catalytic activity for oxygen reduction, and high chemical stability in reducing atmosphere is strontium-doped lanthanum ferrite (LSF) or La$_{1-x}$Sr$_x$FeO$_3$. Presently, the search for superior SOFC cathode or oxygen membrane material is to a large degree based on a trial-and-error approach. An understanding of the detailed mechanism of the oxygen reduction process over model cathode (or membrane) materials, such as LSF, would enable researchers to make more qualified guesses on what materials to choose and how to optimize these by, e.g., partial substitution of the elements. In this study, different reaction mechanisms for the oxygen reduction on LSF are described and compared to experimental investigations carried out on a thin film.

The oxygen transport in a MIEC is determined by the oxygen exchange over the gas-solid interface and diffusion of both oxide ions and electrons/holes in the bulk. The oxygen transport is generally limited by the surface exchange process or by the bulk diffusion, depending on membrane thickness because the electronic charge carrier density and mobility is large when compared to those of the oxide ion. The ratio of the oxygen chemical diffusion, D_{chem}, to the chemical exchange coefficient, K_{chem}, defines a characteristic length, L_c, ($L_c = D_{chem}/K_{chem}$). This is the sample thickness for which diffusion and surface exchange both determine the transport rate. When L_c is much smaller than the sample thickness, L, the transport rate will be limited by diffusion and for L_c values much larger than the sample thickness, surface exchange limitation will dominate.[1]

Bouwmeester et al.[2] have collected values of L_c reported by various authors for a number of technologically relevant perovskite-type oxides, such as La$_{1-x}$Sr$_x$MnO$_{3-\delta}$, La$_{1-x}$Sr$_x$CoO$_{3-\delta}$ (LSC), LSF, La$_{1-x}$Sr$_x$Co$_{1-y}$Fe$_y$O$_{3-\delta}$ (LSCF), and La$_{1-x}$Sr$_x$Co$_{1-y}$Ni$_y$O$_{3-\delta}$. The characteristic thickness (depending on material, temperature, and oxygen partial pressure) lies in the range from 3 mm for La$_{0.6}$Sr$_{0.4}$Co$_{0.4}$Ni$_{0.6}$O$_{3-\delta}$ to 0.2 μm for La$_{0.5}$Sr$_{0.5}$MnO$_{3-\delta}$ at 900°C and $P_{O_2} = 70$ kPa. For La$_{0.6}$Sr$_{0.4}$FeO$_{3-\delta}$, a L_c value of 0.5 mm at a temperature 1000°C and $P_{O_2} = 6.5$ kPa is reported by Ishigaki et al.[3]

The defect chemistry of LSF together with the transport properties and their dependence on Sr content, oxygen partial pressure, and temperature has been studied by several investigators,[4-15] rendering this class of materials suitable "model materials" for investigation of the surface exchange properties. However, D_{chem} and K_{chem} have typically been measured at sample geometries and in temperature and oxygen partial pressure intervals, where both diffusion and surface exchange affects the oxygen transport.[12-15] In the region of mixed control, it is difficult to simultaneously determine both D_{chem} and K_{chem} with high accuracy because the two parameters affect the experimental signals in much the same way. For example, considering conductivity relaxation or oxygen isotope exchange techniques, the experimental signals are profile curves in time and space, respectively, which flatten by the decrease of both D_{chem} and K_{chem}. This difficulty may be solved by studying thick samples when determining D_{chem} and thin samples (significantly below L_c) for studies of K_{chem}.

In this study, the electrical conductivity relaxation (ECR) technique is used to obtain characteristics of thin (La$_{0.6}$Sr$_{0.4}$)$_{0.99}$FeO$_{3-\delta}$ (LSF64) films. The mechanism of oxygen surface exchange of a film prepared by pulsed laser deposition (PLD) on single-crystal MgO supports is investigated. LSF64 has been preferred above other perovskite materials with similar properties (e.g., LSC and LSCF) because LSF64 is stable under reducing conditions; it has a thermal expansion coefficient significantly closer to that of MgO (than does LSC or LSCF), and we have found that it is relatively easy to deposit LSF64 using PLD. Finally, a number of studies on bulk samples have been reported in the literature, whereby comparison of properties of thin films with bulk samples is possible. Here, a film with a thickness of ~0.66 μm, which is significantly smaller than L_c, is investigated. For such a thickness, the effect of bulk diffusion is negligible (i.e., the response of the sample to a sudden gas change around it is effectively sensitive to the exchange process only, which allows mechanistic information to be deduced).

To avoid reaction between the substrate and the film and to avoid any contribution from the conductivity of the support, the film must be deposited on a substrate with negligible conductivity compared to the film. This is fulfilled with a MgO single-crystal substrate because the conductivity in the investigated temperature range is $<10^{-8}$ S cm^{-1}.

This paper concentrates on investigation of thermodynamic as well as kinetic properties of an LSF64 thin film and discusses possible reaction paths for the oxygen incorporation reaction. In the theory section and Appendix C different reasonable one-, two-, three-, and multistep mechanisms for the incorporation reaction are analyzed and expressions for the expected dependence on defects concentration and P_{O_2} of the exchange coefficient are formulated.

[z] E-mail: peter.hendriksen@risoe.dk

The model predictions are compared to the experimental results obtained from electrical conductivity relaxation on a 657 nm thick film. Further, a simple defect model is presented that is successfully used for calculating the oxygen nonstoichiometry and electron hole mobility of the LSF64 thin film.

Theoretical Considerations

Relaxation technique.— Information on the oxygen surface exchange process of thin films can be obtained from ECR data.[16-18] ECR is based on the measurement of the time variation of the electrical conductivity of the sample after a sudden change in the oxygen partial pressure at constant temperature. For mixed conductors, a change in the oxygen partial pressure results in a change in the charge carrier concentration that will result in a change in the electrical conductivity, which can be monitored experimentally during re-equilibration.[14]

At $t < 0$, the sample is in thermodynamic equilibrium with the ambient gas (δ_0 is the initial equilibrium vacancy concentration in the sample). At $t = 0$, the oxygen partial pressure is suddenly changed. Because the deposited film is much thinner than L_c, transport of oxygen into or out of the material is limited only by the surface exchange process, and the transport equation can be described by a simple mass balance on the sample surface given by[19]

$$A_s K_{\text{chem}}(\delta_0 - \delta_\infty) = - A_g L \frac{d\delta}{dt} \quad [1]$$

where δ_∞ is the nonstoichiometry in the sample after equilibrium is re-established. A_s is the solid-gas interface area. A_g is the geometric area of the thin film. The interface area between solid and gas is larger than the A_g of the film due to the roughness of the surface of the film. Because the ratio between the geometric area and the area of the interface between solid and gas is an unknown parameter for the sample considered here, it has been chosen to assume $A_g = A_s$ as is usually done for these types of studies. (It should be noted though that if $A_s/A_g \neq 1$, then it affects the absolute value derived for K_{chem} but not its temperature or P_{O_2} dependence, which are the more significant features when trying to deduce mechanistic information.)

In Eq. 1, it is assumed that the surface exchange reaction follows a first-order reaction. The chemical exchange coefficient is defined by

$$\frac{K_{\text{chem}}}{L} = \lim_{\delta \to \delta_\infty} \frac{r}{\delta - \delta_\infty} \quad [2]$$

where $r = -d\delta/dt$ is the reaction rate at the surface. As discussed by Maier[20,21] and Adler et al.[22] based on transition state theory, the net rate of an elementary reversible reaction, r, is equal to the difference in the forward and reverse reaction rate.

For the incorporation of oxygen

$$\frac{1}{2}O_2 + V_O^{\cdot\cdot} \leftrightarrow O_O^X + 2h^\cdot \quad [3]$$
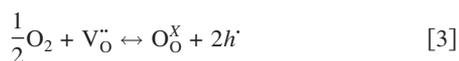
one can express the reaction rate based on transition-state theory, if one can assume that the incorporation of oxygen is an elementary reaction

$$r = k[P_{O_2}^{1/2}\delta e^{-(\Delta G_f/RT)} - (3 - \delta)(x - 2\delta)^2 e^{-\Delta G_b/RT}] \quad [4]$$

Under oxidizing conditions, the current is carried by electron holes with concentration $p = x - 2\delta$. ΔG_f and ΔG_b are the difference between Gibbs free energy of the reactant/transition state in the forward direction and the difference between Gibbs free energy of the product/transition state in the backward direction, respectively. The reaction Gibbs free energy is $\Delta G_r = \Delta G_f - \Delta G_b$.

Adler et al.[22] have shown that, based on the irreversible thermodynamics, r can be stated in the exponential form as $r = R_0[1 - \exp(-\Lambda/RT)]$, where R_0 is the oxygen exchange rate in the limit of equilibrium and is proportional to the product of the concentration of species on the left-hand side of the reaction ($R_0 = kP_{O_2}^{1/2}\delta$).

The proportionality coefficient depends on the reaction symmetry parameter, shift in free energy of reaction described by Adler et al.,[22] and driving force, Λ. The driving force Λ is the difference in the chemical potential of the reactants and products.

For the incorporation of oxygen in vacancies one can express the driving force Λ as

$$- \Lambda = \mu_{O_O^X} + 2\mu_{h^\cdot} - \mu_{V_O^{\cdot\cdot}} - 1/2\mu_{O_2} \quad [5]$$

where $\mu_i = \mu_i^0 + RT \ln(f_i C_i)$ is the chemical potential of species i. f_i and C_i are activity coefficient and concentration for the same species, respectively.

Rearrangement of Eq. 5 yields

$$- \Lambda = \Delta G^0 + \Delta G^{\text{ex}} + RT \ln\left[\frac{(3 - \delta)(x - 2\delta)^2}{P_{O_2}^{1/2}\delta}\right] \quad [6]$$

where $\Delta G^0 = \mu_{O_O^X}^0 + 2\mu_{h^\cdot}^0 - \mu_{V_O^{\cdot\cdot}}^0 - (1/2)\mu_{O_2}^0$ and $\Delta G^{\text{ex}} = RT \ln(f_{O_O^X}f_{h^\cdot}^2/f_{V_O^{\cdot\cdot}}f_{O_2}^{1/2})$ are reaction Gibbs energy and excess free energy, respectively. For an ideal solution, the excess Gibbs free energy, ΔG^{ex} is zero.

At equilibrium, Eq. 6 thus reduces to

$$0 = \Delta G_{\text{eq}}^0 + \Delta G_{\text{eq}}^{\text{ex}} + RT \ln\left[\frac{(3 - \delta_\infty)(x - 2\delta_\infty)^2}{P_{O_2}^{1/2}\delta_\infty}\right] \quad [7]$$

Subtraction of Eq. 7 from Eq. 6 yields

$$- \Lambda = \Delta G^0 - \Delta G_{\text{eq}}^0 + \Delta G^{\text{ex}} - \Delta G_{\text{eq}}^{\text{ex}} + RT \ln\left[\frac{\delta_\infty(3 - \delta)(x - 2\delta)^2}{\delta(3 - \delta_\infty)(x - 2\delta_\infty)^2}\right] \quad [8]$$

The term $\Delta G^0 - \Delta G_{\text{eq}}^0 + \Delta G^{\text{ex}} - \Delta G_{\text{eq}}^{\text{ex}}$ is a complex function of the reactants and products concentration and thus complicates the study of the effect of reaction parameters (concentration, temperature, and pressure) on the exchange rate and investigation of the mechanism of a complex reaction. This term can, in the limit of small deviation from the equilibrium, be assumed to be zero when the variation of the nonstoichiometry (or driving force Λ) is small. In such a situation, Eq. 8 reduces to

$$- \Lambda = RT \ln\left[\frac{\delta_\infty(3 - \delta)(x - 2\delta)^2}{\delta(3 - \delta_\infty)(x - 2\delta_\infty)^2}\right] \quad [9]$$

By inserting Eq. 9 into the reaction rate $r = R_0[1 - \exp(-\Lambda/RT)]$, one obtains the net reaction rate

$$r = - \frac{d\delta}{dt} = kP_{O_2}^{1/2}\delta\left[1 - \frac{(3 - \delta_\infty)(x - 2\delta)^2}{(3 - \delta)(x - 2\delta_\infty)^2}\right] \quad [10]$$

where the reaction constant k belongs to the forward reaction. Assuming that the fraction of lattice oxygen, O_O^X remains constant equal to 3, further simplification of Eq. 10 yields

$$r = kP_{O_2}^{1/2}\frac{(x^2 - 4\delta\delta_\infty)}{(x - 2\delta_\infty)^2}(\delta - \delta_\infty) \quad [11]$$

Applying the definition of K_{chem} one finds

$$\frac{K_{\text{chem}}}{L} = kP_{O_2}^{1/2}\frac{x + 2\delta_\infty}{x - 2\delta_\infty} \quad [12]$$

Equation 12, which can be applied to relaxations close to equilibrium, shows that K_{chem} depends directly on P_{O_2}, defect concentrations, and on temperature via the temperature dependence of the reaction rate constant (secondarily also via the temperature dependence of δ_∞). In the section on "Thermodynamic Considerations," it will be shown that the last term in Eq. 12 defines a thermodynamic property, namely, the thermodynamic factor for vacancies.

By measurement of K_{chem} as a function of P_{O_2} at different temperatures, one can compare the experimental data to the model (Eq. 12). K_{chem} can be deduced from measurement of the time depen-

dence of the electrical conductivity after a step change in P_{O_2} around the sample. The connection between K_{chem} and total electrical conductivity can be obtained by solving Eq. 1. In the limit of small displacements from equilibrium, one can assume that K_{chem} is independent of δ and Eq. 1 can be integrated to obtain the solution for δ

$$\frac{\delta - \delta_\infty}{\delta_0 - \delta_\infty} = e^{-K_{chem}(t/L)} \qquad [13]$$

As noted before, a change in the oxygen-ion concentration can be related to the change in the total conductivity. The total conductivity is the sum of the ionic and electronic conductivities. Bahteeva et al.[6] has measured a total conductivity of 283 S/cm at $P_{O_2} = 1$ atm and an oxygen-ion conductivity of 0.14 S/cm for $La_{0.6}Sr_{0.4}FeO_{3-\delta}$ at a temperature of 800°C on a bulk sample. Because the ionic conductivity is smaller than the electronic conductivity by several orders of magnitude, the total conductivity can with good approximation be considered equal to the electronic conductivity. The total electrical conductivity, σ, is given by the sum of the partial conductivities of electrons and holes. Under oxidizing conditions ($0.001 < P_{O_2} < 1$ atm), the current is carried mainly by electron holes[5,6,10-12] and the resulting expression for the electrical conductivity is

$$\sigma = \frac{F\mu}{V_m} p \qquad [14]$$

where μ and p are the mobility and the concentration of electron holes, respectively. V_m is the molar volume of LSF64, and F is the Faraday constant.

Because of electroneutrality and site conservation, the concentrations of species cannot change independently of each other. For $La_{1-x}Sr_xFeO_{3-\delta}$, the equations for site and charge balance are

$$\delta + C_O = 3$$

$$x = p + 2\delta \qquad [15]$$

where C_O is the fraction of lattice oxygen O_O^X in dimensionless form (see also next section). Combination of Eq. 13-15 results in

$$\frac{\sigma - \sigma_\infty}{\sigma_0 - \sigma_\infty} = e^{-K_{chem}(t/L)} \qquad [16]$$

The experimental conductivity relaxation data can be fitted to Eq. 16 using σ_0, σ_∞, and the chemical exchange coefficient, K_{chem}, as the fitting parameters. σ_0, σ_∞ are the total conductivities prior to the gas change (at time equal to zero) and after the gas change (after long time) when the equilibrium has been re-established, respectively.

Thermodynamic considerations.— In order to study oxygen exchange kinetics on the surface, it is first necessary to know the thermodynamic properties of the thin film, such as concentration of oxygen vacancy (nonstoichiometry) as a function of temperature and oxygen partial pressure. We introduce a set of thermodynamic relationships between the oxygen vacancy concentration, electron hole concentration, thermodynamic factor, and total electrical conductivity.

In order to account for the defect chemistry of LSF, a simple model has been chosen. The variations of the electrical properties with oxygen partial pressure (in the considered P_{O_2} interval) can be analyzed assuming p-type charge carriers and oxide-ion vacancies as the predominant defects. In Kröger–Vink notation, the overall exchange reaction at the gas/film interface can be written as

$$\frac{1}{2}O_2 + V_O^{\cdot\cdot} \leftrightarrow O_O^X + 2h^{\cdot} \qquad [17]$$
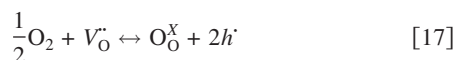
where $V_O^{\cdot\cdot}$ and $h^{\cdot}$ denote an oxygen vacancy and an electron hole, respectively. O_O^X is an oxide ion on an oxide-ion lattice site.

Reaction 17 considers only the number of electronic defects. There is no specification about the number of available sites; more-

over, the possibility of n-type charge carriers is neglected. This is a simplification relative to the generally applied model of the defect chemistry of LSF, where also n-type defects are considered and the charges are assumed to be localized on the iron sites.[9-14] The advantage of this simplification is the possibility to write down a closed-form expression for the defect concentration as a function of P_{O_2}. The model is thus only applicable at high oxygen partial pressures, where the main charge carrier is electron holes and the concentration of electron holes is relatively large. As shall be shown, it accounts very well for the variation in the electrical conductivity with temperature and oxygen partial pressure in the intervals studied here.

The oxygen pressure dependence of δ_∞ may under assumption of ideal behavior be derived by applying the mass-action law on Eq. 17

$$K_{eq} = \frac{(3 - \delta_\infty)(x - 2\delta_\infty)^2}{P_{O_2}^{1/2}\delta_\infty} \qquad [18]$$

In this study, the oxygen nonstoichiometry, δ_∞ remains small (<0.11) and the approximation $O_O^X = 3 - \delta_\infty \approx 3$ is applied

$$K_{eq} = \frac{3(x - 2\delta_\infty)^2}{P_{O_2}^{1/2}\delta_\infty} \qquad [19]$$

This simplification is convenient in order to obtain a simple analytical expression for δ_∞. The concentration of oxygen vacancies or electron holes can be obtained by solving Eq. 19 for δ_∞

$$x - 2\delta_\infty = \frac{1}{12}K_{eq}P_{O_2}^{1/2}\left(\sqrt{1 + \frac{24x}{K_{eq}P_{O_2}^{1/2}}} - 1\right) \qquad [20]$$

The square-root term in Eq. 20 defines a special thermodynamic property, namely, the thermodynamic factor for vacancies. The chemical diffusion coefficient, D_{chem}, can be related to either the vacancy diffusion coefficient, D_V, by the thermodynamic factor for vacancies, Γ_V, or to the oxygen diffusion coefficient, D_O, by the thermodynamic factor for oxygen, Γ_O, according to $D_{chem} = \Gamma_V D_V = \Gamma_O D_O$.[15] Since the vacancy conductivity is the same as the oxygen ion conductivity, one can write $D_V\delta = D_O(3 - \delta)$ where $(3 - \delta)$ is the dimensionless concentration of oxide ions (fraction of lattice oxygen).

The thermodynamic factor for vacancies is defined as[15]

$$\Gamma_V = -\frac{1}{2}\frac{d\ln(P_{O_2})}{d\ln(\delta)} \qquad [21]$$

and the thermodynamic factor for oxide ions as

$$\Gamma_O = \frac{1}{2}\frac{d\ln(P_{O_2})}{d\ln(C_O)} \qquad [22]$$

The two thermodynamic factors are thus related by

$$\frac{\Gamma_O}{3 - \delta} = \frac{\Gamma_V}{\delta} \qquad [23]$$

By differentiation of Eq. 19, one can show that

$$\Gamma_V = \sqrt{1 + \frac{24x}{K_{eq}P_{O_2}^{1/2}}} \qquad [24]$$

which is exactly the square-root term in Eq. 20. By combining Eq. 14 and 20, the electrical conductivity can be written

$$\sigma = \frac{F\mu}{V_m}\frac{1}{12}K_{eq}P_{O_2}^{1/2}\left(\sqrt{1 + \frac{24x}{K_{eq}P_{O_2}^{1/2}}} - 1\right) = \frac{F\mu}{V_m}\frac{1}{12}K_{eq}P_{O_2}^{1/2}(\Gamma_V - 1) \qquad [25]$$

It is evident from Eq. 25 that the equilibrium constant of the overall reaction and the electron hole mobility, μ, can be evaluated from the experimental measurements of electrical conductivity as a function of oxygen partial pressure at any temperature by fitting this equation to the experimental results (under the assumption that both K_{eq} and

μ are independent of P_{O_2}). The two parameters K_{eq} and μ can be used to calculate the thermodynamic factor and the concentration of vacancies or electron holes from Eq. 24 and 20, respectively.

From Eq. 25, the slope of the curve of σ vs P_{O_2} in a log-log plot is given by

$$\frac{d \log \sigma}{d \log P_{O_2}} = \frac{1}{4} - \frac{1}{4\Gamma_V} \qquad [26]$$

Equation 26 expresses the local slope of $\log \sigma$ vs $\log P_{O_2}$, $n = d(\log \sigma)/d(\log P_{O_2})$ as a function of only one variable, namely, $\Gamma_V (T, P_{O_2})$. The slope, n, will vary between $0 < n < 1/4$ (note that $\Gamma_V > 1$).

One can easily show that the nonstoichiometry as well as electrical conductivity can be expressed as a function of the thermodynamic factor by the following equations

$$\delta_\infty = \frac{x(\Gamma_V - 1)}{2(\Gamma_V + 1)} \qquad [27]$$

$$\sigma = \frac{2xF\mu}{V_m(\Gamma_V + 1)} \qquad [28]$$

Equations 27 and 28 are useful because the conductivity and concentration of the defects (vacancy/hole) can be described as functions of the thermodynamic factor only, without considering the temperature and oxygen partial pressure.

Kinetic considerations.— The reaction of oxygen with the film at the gas-solid interface is, in general, a complex process that consists of several elementary reactions involving O_2 transport from gas phase to surface, adsorption on the surface, dissociation and charge transfer, and finally, incorporation into the surface layer. Several species can occur as intermediates for the exchange reaction [e.g., $(O_2)_{ads}$, $(O_2)^-_{ads}$, O^-_{ads}, and $(O_2)^{-2}_{ads}$].[23] The series of elementary steps that can vary from material to material are not yet well understood, and a significant number of mechanisms have been suggested by different authors.[14,19-21,24-27]

In the following, possible reasonable one-, two-, and three-step reaction mechanisms for the incorporation of oxygen in LSF are discussed.

One-step mechanism.— In the simplest possible model, one can assume that the surface reaction, Eq. 17 is itself an elementary reaction corresponding to direct incorporation of oxygen into vacancies with the simultaneous oxidation of B ions (formation of electron holes on the iron site).

The kinetics can be described by standard chemical reaction rate expression involving a reaction rate constant, k, and species partial pressures or concentrations

$$r = -\frac{d\delta}{dt} = k\left[P_{O_2}^{1/2}\delta - \frac{3(x - 2\delta)^2}{K_{eq}} \right] \qquad [29]$$

k is the temperature-dependent reaction rate constant for the forward reaction.

At equilibrium (for $t \to \infty$), the reaction rate approaches zero and we may write

$$0 = k\left[P_{O_2}^{1/2}\delta_\infty - \frac{3(x - 2\delta_\infty)^2}{K_{eq}} \right] \qquad [30]$$

By subtracting Eq. 30 from Eq. 29 and using Eq. 24 and 27, the rate of the exchange reaction can be written as

$$-\frac{d\delta}{dt} = kP_{O_2}^{1/2}\Gamma_V\left(1 - \frac{\delta - \delta_\infty}{\delta_\infty}\frac{(\Gamma_V - 1)^2}{4\Gamma_V} \right)(\delta - \delta_\infty) \qquad [31]$$

By combination of Eq. 1 and 31 one finds

$$\frac{K_{chem}}{L} = kP_{O_2}^{1/2}\Gamma_V\left(1 - \frac{\delta - \delta_\infty}{\delta_\infty}\frac{(\Gamma_V - 1)^2}{4\Gamma_V} \right) \qquad [32]$$

For small perturbations (small P_{O_2} step, $\delta \approx \delta_\infty$), the expression for K_{chem} reduces to

$$\frac{K_{chem}}{L} = kP_{O_2}^{1/2}\Gamma_V \qquad [33]$$

By using Eq. 27, the thermodynamic factor for vacancies can be expressed in terms of the vacancy concentration [$\Gamma_V = (x + 2\delta)/(x - 2\delta)$]. It is observed that Eq. 33 is identical to Eq. 12. In a situation when the departure from equilibrium is not small, there will be an error on K_{chem} that depends on $\delta - \delta_\infty$ or alternatively on the P_{O_2} step change and thermodynamic factor. In Appendix B, we investigated which experimental conditions must be fulfilled for the "approach to equilibrium" assumption to apply.

It can be observed from Eq. 33 that the expression for K_{chem} is a product of two terms. The first term is a kinetic term (surface exchange rate), and the second term reflects an equilibrium property (thermodynamic factor). The chemical surface exchange coefficient, K_{chem} can be converted to the surface exchange coefficient, k_V, via the thermodynamic factor according to
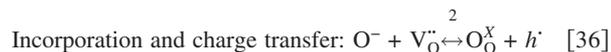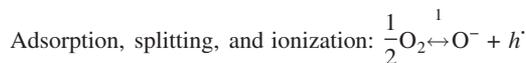
$$K_{chem} = k_V\Gamma_V \qquad [34]$$

Note that k_V reflects the kinetics (or surface exchange reaction) while K_{chem} reflects both kinetic and thermodynamic via Γ_V. In analogy with the chemical diffusion coefficient (D_{chem}), K_{chem} can be related to either the vacancy surface exchange coefficient, k_V, or to the oxygen surface exchange coefficient, k_O by $K_{chem} = \Gamma_V k_V = \Gamma_O k_O$. The two surface exchange coefficients are related by $k_V\delta = k_O(3 - \delta)$. k_O is the surface exchange coefficient one would measure in a $^{16}O/^{18}O$ tracer diffusion experiment.

Combination of Eq. 33 and 34 yields

$$\frac{k_V}{L} = kP_{O_2}^{1/2} \text{ or } \frac{k_O}{L} = kP_{O_2}^{1/2}\frac{\delta_\infty}{3 - \delta_\infty} \qquad [35]$$

Equation 35 shows that the vacancy surface exchange coefficient, k_V, must be proportional to the square root of oxygen partial pressure if the oxygen incorporation reaction is a single-step process described by Eq. 17. The described mechanism begins with half an oxygen molecule. Because the physical reacting species is an oxygen molecule, the remaining oxygen atom should, in principle, also be accounted for. Assuming the reaction to occur via Eq. 17 implicitly requires that the second atom reacts by some process with the characteristics that it does not affect the rate of the reaction (Eq. 17).

Two-step mechanism.— For the sake of illustration, a possible two-step mechanism for the oxygen incorporation is considered.[25] Other possible two-step reaction mechanisms can be found in Appendix C

$$\text{Adsorption, splitting, and ionization: } \frac{1}{2}O_2 \overset{1}{\leftrightarrow} O^- + h^\cdot$$

$$\text{Incorporation and charge transfer: } O^- + V_O^{\cdot\cdot} \overset{2}{\leftrightarrow} O_O^X + h^\cdot \qquad [36]$$

In the proposed two-step mechanism, we assume that the first step is adsorption, splitting, and ionization of oxygen to O^- on the surface, and consequent formation of an electron hole (the oxygen molecule can exchange one of the atoms at the surface). The second step is the ion transfer by the incorporation of O^- into a vacancy and formation of another electron hole. This is illustrated further in Fig. 1.

According to the steady-state approximation,[28] the concentration of intermediate O^- remains practically constant during the course of the reaction, so that to a good approximation the rate of change of O^- can be set equal to zero
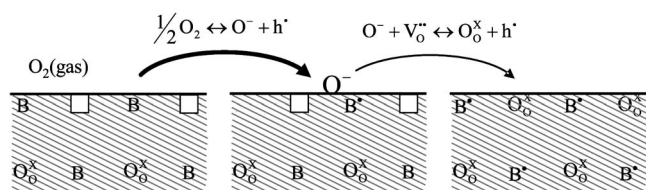
Figure 1. Mechanistic image of a two-step incorporation reaction.

$$\frac{d[O^-]}{dt} = k_1 P_{O_2}^{1/2} - k_{-1}[O^-](x - 2\delta) - k_2[O^-]\delta + 3k_{-2}(x - 2\delta) = 0$$

[37]

where k_i and k_{-i} are the rate constants of the forward and backward reactions of the related steps.

The concentration of O^- can be obtained by solving Eq. 37 for $[O^-]$

$$[O^-] = \frac{k_1 P_{O_2}^{1/2} + 3k_{-2}(x - 2\delta)}{k_{-1}(x - 2\delta) + k_2\delta}$$

[38]

The consumption of vacancies can be expressed by

$$-\frac{d\delta}{dt} = k_2[O^-]\delta - 3k_{-2}(x - 2\delta)$$

[39]

By inserting $[O^-]$ from Eq. 38 into Eq. 39, one obtains

$$-\frac{d\delta}{dt} = \frac{K_{eq}\left[P_{O_2}^{1/2}\delta - \dfrac{3(x - 2\delta)^2}{K_{eq}} \right]}{\dfrac{x - 2\delta}{k_{-2}} + \dfrac{K_2^{eq}}{k_{-1}}\delta}$$

[40]

where K_1^{eq} and K_2^{eq} are the equilibrium constants of the elementary reactions and $K_{eq} = K_1^{eq}K_2^{eq}$ is the equilibrium constant of the overall reaction.

The reaction rate at equilibrium approaches zero

$$0 = \frac{K_{eq}P_{O_2}^{1/2}\left[\delta_\infty - \dfrac{3(x - 2\delta_\infty)^2}{K_{eq}P_{O_2}^{1/2}} \right]}{\dfrac{x - 2\delta_\infty}{k_{-2}} + \dfrac{K_2^{eq}}{k_{-1}}\delta_\infty}$$

[41]

By subtracting Eq. 41 from Eq. 40 and applying the definition of K_{chem}, one obtains an expression for K_{chem}

$$\frac{K_{chem}}{L} = \frac{K_{eq}P_{O_2}^{1/2}\Gamma_V}{[(x - 2\delta_\infty)/k_{-2}] + (K_2^{eq}/k_{-1})\delta_\infty}$$

[42]

The resulting expression for k_V is

$$\frac{k_V}{L} = \frac{K_{eq}P_{O_2}^{1/2}}{[(x - 2\delta_\infty)/k_{-2}] + (K_2^{eq}/k_{-1})\delta_\infty}$$

[43]

If the rate of the first reaction is slow compared to the second reaction, the first step will be rate determining and the second step close to equilibrium. In this situation, Eq. 43 reduces to

$$\frac{k_V}{L} = \frac{k_1 P_{O_2}^{1/2}}{\delta_\infty} \quad \text{or} \quad \frac{k_O}{L} = \frac{k_1 P_{O_2}^{1/2}}{3 - \delta_\infty}$$
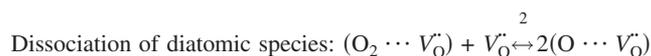
[44]

In this case, one should thus observe that k_V is proportional to the square root of oxygen partial pressure and inversely proportional to the vacancy concentration. Because the vacancy concentration, $\delta_\infty \propto P_{O_2}^{-(1/2\Gamma_V)}$, the overall $P_{O_2}^n$ dependency of k_V has the order $n = 1/2(1 + 1/\Gamma_V)$, which varies between 0.5 and 1.

In the case where the second step is the rate-determining step (RDS) and the first step is assumed to be in equilibrium, it can be shown that

$$\frac{k_V}{L} = \frac{k_{-2}K_{eq}P_{O_2}^{1/2}}{x - 2\delta_\infty} \quad \text{or} \quad \frac{k_O}{L} = \frac{k_{-2}K_{eq}P_{O_2}^{1/2}}{x - 2\delta_\infty}\frac{\delta_\infty}{3 - \delta_\infty}$$

[45]

Here, the exchange coefficient is again proportional to the square root of oxygen partial pressure but inversely proportional with the hole concentration. The hole concentration, $x - 2\delta_\infty \propto P_{O_2}^{(1/4)-(1/4\Gamma_V)}$ has a positive exponent; consequently, the overall $P_{O_2}^n$ dependency of k_V has order $n = 1/4(1 + 1/\Gamma_V)$, where n is in the range $1/4 < n < 1/2$.

Three-step mechanism.— A number of possible three-step reaction mechanisms for incorporation of oxygen in the lattice can be postulated (Appendix C). As an example, we consider here an incorporation reaction (Eq. 17) consisting of three elementary steps

$$\text{Adsorption of } O_2 \text{ on a vacancy: } O_2 + V_O^{\cdot\cdot} \overset{1}{\leftrightarrow} (O_2 \cdots V_O^{\cdot\cdot})$$

$$\text{Dissociation of diatomic species: } (O_2 \cdots V_O^{\cdot\cdot}) + V_O^{\cdot\cdot} \overset{2}{\leftrightarrow} 2(O \cdots V_O^{\cdot\cdot})$$

$$\text{Incorporation/charge transfer: } (O \cdots V_O^{\cdot\cdot}) \overset{3}{\leftrightarrow} O_O^X + 2h^{\cdot}$$

[46]

The first step is adsorption of molecular oxygen on a vacant site at the gas/solid interface. We assume that adsorption of oxygen takes place at the oxide vacancies on the film surface. This assumption is consistent with the experimental measurements of surface exchange coefficient presented in the "Results and Discussion" section, and we shall return to this later. The second step is the dissociation of the adsorbed diatomic, $(O_2 \cdots V_O^{\cdot\cdot})$ to neutral monoatomic oxygen $(O \cdots V_O^{\cdot\cdot})$. Here, the dissociation requires a neighbor vacant site to interact with the adsorbed oxygen molecule. In this step, the adsorbed diatomic oxygen, $(O_2 \cdots V_O^{\cdot\cdot})$ migrates over the surface until it meets another vacant site. The dissociation of $(O_2 \cdots V_O^{\cdot\cdot})$ to $(O \cdots V_O^{\cdot\cdot})$ can also happen in two steps according to Reaction 11 in Appendix C. And finally, the third step is the incorporation of adsorbates (neutral monoatomic oxygen in a vacancy) into the film and simultaneously formation of electron holes.

Application of the steady-state approximation to the mechanism leads to the following expression of the chemical exchange coefficient as discussed in Appendix A

$$\frac{K_{chem}}{L} = \frac{P_{O_2}\delta_\infty\Gamma_V}{(1/k_{-3}K_{eq})P_{O_2}^{1/2}\delta_\infty + (1/4k_1)\delta_\infty + (1/4k_2K_1^{eq})}$$

[47]

where K_1^{eq}, K_2^{eq}, and K_3^{eq} are the equilibrium constants of the elementary reactions and $K_{eq} = \sqrt{K_1^{eq}K_2^{eq}}K_3^{eq}$ is the equilibrium constant of the overall reaction.

Combination of Eq. 34 and 47 leads to

$$\frac{k_V}{L} = \frac{P_{O_2}\delta_\infty}{\dfrac{1}{k_{-3}K_{eq}}P_{O_2}^{1/2}\delta_\infty + \dfrac{1}{4k_1}\delta_\infty + \dfrac{1}{4k_2K_1^{eq}}}$$

[48]

Equation 48 can be reduced to a simple expression if one of the three steps in the mechanism scheme (Eq. 46) is the RDS, whereas the others are in equilibrium.

1. If one supposes that the first step is RDS and the two others are in equilibrium, then it can be shown that

$$\frac{k_V}{L} = 4k_1 P_{O_2} \quad \text{or} \quad \frac{k_O}{L} = 4k_1 P_{O_2}\frac{\delta_\infty}{3 - \delta_\infty}$$

[49]

In this case, k_V is first order in oxygen partial pressure ($k_V \propto P_{O_2}^n, n = 1$).

Equation 49 for the oxygen exchange coefficient is effectively identical to $k_O \propto P_{O_2}\delta_\infty$, which was suggested by ten Elshof et al.[14] from a study where k_O was measured on a bulk $La_{0.6}Sr_{0.4}FeO_{3-\delta}$ sample. The data of ten Elshof et al. show that the overall $P_{O_2}^n$ dependency of k_O was of order $0.65 < n < 0.84$ (the value of n depends on temperature and oxygen partial pressure). Therefore, it was concluded that the RDS involved one molecular oxygen and one vacancy. They observed a linearlike correlation by plotting the ratio k_O/P_{O_2} vs δ_∞, which supports the RDS, must be step 1 in the mechanism scheme (Eq. 46).

2. If the second step is the RDS and the two others are at equilibrium, then the expressions for the exchange coefficients will be

$$\frac{k_V}{L} = 4k_2 K_1^{eq} P_{O_2}\delta_\infty \text{ or } \frac{k_O}{L} = 4k_2 K_1^{eq} P_{O_2}\frac{\delta_\infty^2}{3-\delta_\infty} \qquad [50]$$

Here, the k_V is proportional with both oxygen partial pressure and vacancy concentration, which itself has a negative exponent in pressure, consequently the overall $P_{O_2}^n$ dependency of k_V is of order $0.5 < n < 1$.

3. If the third step is RDS and the two others are at equilibrium, then one finds

$$\frac{k_V}{L} = k_{-3}K_{eq}P_{O_2}^{1/2} \text{ or } \frac{k_O}{L} = k_{-3}K_{eq}P_{O_2}^{1/2}\frac{\delta_\infty}{3-\delta_\infty} \qquad [51]$$

In this case, k_V is of order 1/2 in the oxygen partial pressure.

The analyses of the three cases suggest that the order of the surface exchange coefficient, k_V in oxygen partial pressure can neither be <0.5 nor >1 for the assumed mechanism. There are a lot of other possibilities for mechanisms. A number of different reasonable ones are treated and summarized in Appendix C. The order of the exchange coefficient in P_{O_2} is calculated if different elementary reactions are taken to be RDS. For all the mechanisms considered in Appendix C, it holds that the molecularity is ≤ 2. The elementary reaction $O_2 + 2V_O^{\cdot\cdot} -> 2O_x + 4h$ is thus not considered, as the number of molecular entities that participate in the reaction is three and is thus considered improbable.

Under the assumption that a single reaction is RDS, the equation for k_V can in all cases be expressed by a power-law kinetic equation

$$\frac{k_V}{L} \propto P_{O_2}^m \delta_\infty^n (x - 2\delta_\infty)^t \qquad [52]$$

which is consistent with Eq. 16 derived in Merkle and Maier.[24]

The exponents m, n, and t can be determined by best fitting of the experimental data by the above model.

Experimental

Deposition of thin films with PLD requires a target of the same composition as the thin film. This target was prepared using a standard synthesis method and ceramic procedure: $(La_{0.6}Sr_{0.4})_{0.99}FeO_3$ (LSF64) powder was prepared using the glycine nitrate process. Stock solutions of $La(NO_3)_3 \cdot 6H_2O$ (Alfa Aesar, 99%), $Sr(NO_3)_2$ (Alfa Aesar, 99%), and $Fe(NO_3)_3 \cdot 9H_2O$ (Alfa Aesar, +98%) in water were prepared. The concentration of the solutions were determined by a thermogravimetric method. The solutions were mixed in the stoichiometric correct amount as to give LSF64. Glycine (Alfa Aesar, 99.9%) was added, such that the stoichiometric amount of glycine to that of the stoichiometric amount of the nitrates was 0.548. The solution was subsequently dried to form a gel state. On further heating, the resultant viscous resin ignited and underwent self-sustaining combustion within a few seconds, producing an ash composed of the oxide product. This powder was calcined at 900°C for 24 h followed by ballmilling in ethanol for one week and drying. The powder was pressed uniaxially in a die with a diameter of 49 mm using a pressure of ~10 MPa. The sample was subsequently placed in a latex container that was evacuated, and then isostatically pressed at 325 MPa. Finally, the sample was sin-

tered in air at 1200°C for 20 h. Prior to deposition experiments the targets were polished with 4000 mesh SiC. The target size was ~30 mm after sintering.

A UV KrF excimer pulsed laser system was used for deposition on MgO single crystal (100). The laser was operated at wavelength of 248 nm, pulsed duration of 20 ns, fluence of 4 J/cm², frequency of 40 Hz, and a target-to-substrate distance of 88 mm was used. The substrate was heated to a temperature of 750°C. The vacuum chamber with oxygen as processing gas was evacuated by a turbomolecular pump to a pressure of 10 Pa. Under these conditions, a deposition rate of ~7 nm/min was obtained.[29] The deposition was carried out with a deposition time of 100 min. In order to avoid breaking the film/substrate and to get good statistics for the film thickness determination, a nondestructive method was used. The film thickness was determined by energy dispersive spectrometry with help of scanning electron microscopy (SEM) using Monte Carlo simulations as described by Mosleh et al.[29]

The conductivity relaxation measurements were made on a 16 mm² sample with thickness of 657 nm in the temperature range 650–800°C. The sample was placed inside a 30 cm long closed-end quartz tube with a diameter of 2.5 cm. The oxygen partial pressure in the quartz tube can be controlled by varying the flow rates of different gases. In the present study, flows of oxygen and nitrogen were used for preparing oxygen partial pressures in the range of 1–0.003 atm. The oxygen partial pressure steps were targeted such that $(P_{O_2})_f/(P_{O_2})_i \leq 2$ where $(P_{O_2})_f$ and $(P_{O_2})_i$ are the final and initial oxygen partial pressures, respectively. A zirconia-based electrochemical cell was used for measuring the oxygen partial pressure in the carrier gas mixture (O_2/N_2). The quartz tube creates an empty reactor volume of 147 mL. To minimize the total volume of the glass reactor, a ceramic tube and a thermocouple was brought inside the reactor. In this situation, the characteristic time constant for the reactor is $\tau = (T_0/T)(V/Q_0)$, where Q_0 (250 mL/min) is the total flow rate measured at standard temperature and pressure (room temperature T_0 and 1 atm pressure). Because $T > 650°C$ and the available volume $V < 150$ mL, one finds $\tau < 12$ s (the reactor response in all the performed relaxations is, in practice, <12 s as the gas inlet is placed close to the sample). In all cases, the time constant for changing the oxygen pressure in the reactor is several orders of magnitude lower than the relaxation time of the sample investigated in this study.

Two parallel gold wires were fixed on the surface, and platinum paste was applied to ensure sufficient current collection. A constant current of 0.5 mA was used, and the voltage across the sample was measured with a voltmeter every 3 s. As the substrate resistance is significantly higher than that of the film, the current is assumed to only flow through the film.

In this study, the nominal composition $(La_{0.6}Sr_{0.4})_{0.99}FeO_{3-\delta}$ has been synthesized and used for the investigations. In the literature stoichiometric composition (e.g., $La_{0.6}Sr_{0.4}FeO_{3-\delta}$) are often investigated. However, from simple practically laboratory reasons (purity of powders, synthesis method, accuracy upon weighing, etc.) there will be, in practice for such materials, some deviation from a perfect A/B ratio of one. This will result in either formation of cation vacancies or small amounts of secondary phases being either La,Sr rich or Fe rich. It is well known that slight deviations from stoichiometry can give rise to altered properties (e.g., surface kinetics and sintering properties). The investigations were carried out on a 1% A-site substoichiometric material (rather than an attempted stoichiometric one) for two reasons: (*i*) One has greatly reduced the risk that La_2O_3 or SrO will form. (These compounds may be detrimental for sample stability/integrity because they are highly reactive to water vapor and CO_2.) And (*ii*) the properties to be studied are much less sensitive to the unavoidable inaccuracies in the stochiometry for this composition than for the stoichiometric one, which should result in better reproducibility.
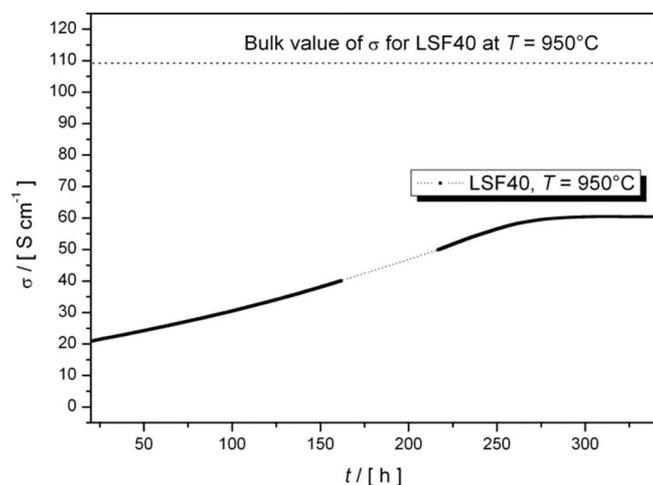
Figure 2. Electrical conductivity, σ, as a function of time, *t*, for the 657 nm thick film of LSF64 in air at 950°C. Also shown is the bulk value of the conductivity at 950°C.

Figure 3. Surface (top) and cross section (bottom) SEM images of the as-deposited LSF64 thin film (657 nm) before (left images) and after heat-treatment (right images) in air at 950°C.

Results and Discussion

Time dependence of the electrical conductivity of thin films.— A short summary of results obtained in a previous work[29] are given below in order to increase the understanding of the underlying physics studied in this paper. In this previous work, thin films of LSF64 of different thicknesses were prepared on MgO single crystals by PLD. The temperature dependence of the conductivity in air for the samples was investigated. It was found that the electrical conductivity of the films does not vary with film thickness when the film exceeds a certain critical thickness of ∼130 nm. It was observed that for samples thinner than the critical thickness, the film dewetted and only partially covered the substrate surface after annealing in air at 950°C. The investigations carried out and reported here are for a film with thickness of 657 nm, which is much thicker than the critical thickness. The electrical behavior of this film was studied in air by the van der Pauw method.[29] Figure 2 shows the conductivity vs time during annealing at 950°C. It is observed that a steady-state value of the conductivity was reached and the conductivity becomes practically independent of time. At 950°C, the oxygen content of the film equilibrates fast; thus, the change in the conductivity over time must be attributed to a change in microstructure and morphology (change in grain size and grain shape). This change of conductivity with time was an irreversible process. The structure of the film before and after the conductivity measurements was investigated by X-ray diffraction (XRD) and by SEM. The XRD measurement shows that the peak positions agree well with those of the target and the position expected for $La_{0.6}Sr_{0.4}FeO_{3-\delta}$ with ICDD data [Code: 82-1961]. No other phases were identified in the diffraction patterns and no peaks that show a reaction between film and substrate. All peaks belong either to LSF64 or MgO (100). The most intense signals originating from the perovskite are located at 2θ = 22.8 and 46.6° and are the (012) and (024) reflections, meaning that the (012) orientation is predominant. A comparison of the XRD data before and after annealing in air at 950°C shows that after heat-treatment the sample still has (012) orientation. The results from the XRD analysis are discussed in more detail in Mosleh et al.[29]

Figure 3 shows the microstructure of the film before and after heat-treatment. The microstructure of the film before heat-treatment shows uniform grain size with triangular grains with very sharp grain boundaries. The film grows with a columnar grain with a porous, rough surface and a faceted structure. Furthermore, it is observed that a tiny space (<10 nm) is present between most of the grains except in the first 100 nm closest to the substrate. The microstructure of the film after heat-treatment shows that the film has
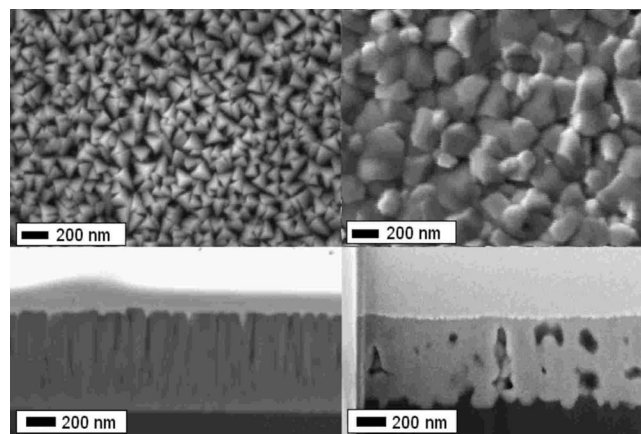
densified, the shape of the grains changed, and the number of grain boundaries decreased. The tiny space between the grains has in the densification process, disappeared. The surface looks flat with closed pores inside the film. The increasing conductivity during the annealing at 950°C is thus a result of the grains sintering together and the tiny space between the grains disappearing. We thus suggest that part of the volume occupied by the tiny spaces between the grains in the preannealed state gives rise to the closed porosity present in the postannealed film.

The XRD data were used to calculate the change in grain size after annealing.[29] Calculations together with SEM images show that during the conductivity measurements at 950°C the grain size increased from ∼85 to ∼169 nm. After this morphology was reached, the conductivity remained constant (60 S/cm); however, the conductivity of the film is still lower than the bulk value (109 S/cm). The cross section of the SEM image of the film shows that after heat-treatment the film contains small closed pores, which reduces the conductivity relative to the bulk value characteristic of a totally dense sample. The difference in conductivity between the film and that reported for bulk does, therefore, not lie in differences in oxygen stoichiometry (will be substantiated in the following) or nanosize effects, but in differences in morphology between film and bulk.

Equilibrium properties.— After the long-term heat-treatment at 950°C, the conductivity was measured at various temperatures and P_{O_2}. Figure 4 shows the variation of electrical conductivity of thin LSF64 film with P_{O_2} in the temperature range of 650–800°C. The solid curves are a best fit of Eq. 25 with μ (electron hole mobility) and K_{eq} as the adjustable parameters (for each temperature) and with the molar volume $V_m = 35.6$ mol/cm³. A lowering of the oxygen partial pressure lowers the electrical conductivity consistent with the *p*-type nature of these mixed ionic and electronic conducting perovskites at high oxygen partial pressures.[12] The electrical conductivity can be well described by Eq. 25. The excellent agreement between the model and the measurements confirms that the assumption of ideal solution behavior and randomly distributed defects is a reasonable approximation for LSF64 (it is only valid as long as the oxygen vacancy concentration is still low). A line with the slope of 1/4 is also illustrated in Fig. 4. It should be noted that the approximation $\sigma \propto P_{O_2}^{1/4}$ is not good in the high-pressure region, where electron hole charge carriers dominate the total conductivity. As described by Eq. 26, the slope of log σ vs log P_{O_2} will vary between $0 < n < 1/4$, depending on temperature and oxygen partial pressure.
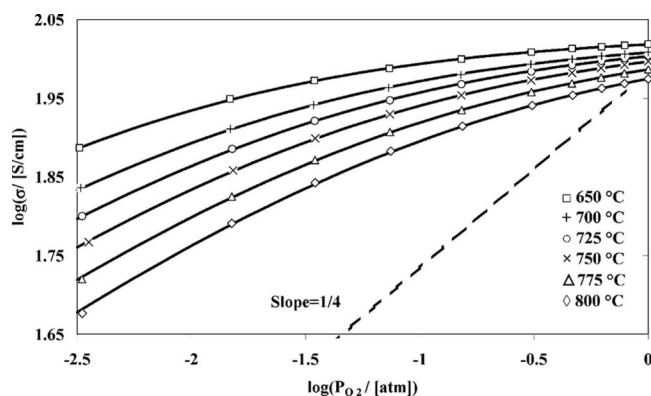
Figure 4. Measured electrical conductivity (symbols), σ, of the thin film of LSF64 as a function of the oxygen partial pressure at different temperatures. The solid lines are the best fit to the measured data using Eq. 25 using the reaction equilibrium constant and the electron hole mobility as fitting parameters. The dashed line shows a slope of 1/4.

The model is observed to account very well for the observed P_{O_2} dependence at all temperatures. The temperature dependence of K_{eq} is given by the thermodynamic quantities ΔH^0 (enthalpy) and ΔS^0 (entropy) for the incorporation reaction,[10] as

$$- \ln K_{eq} = \frac{\Delta H^0}{RT} - \frac{\Delta S^0}{R} \qquad [53]$$

ΔH^0 and ΔS^0 are assumed to be independent of temperature.

Figure 5 shows the fitted values of K_{eq} (left axis) as a function of $1/T$. The values of K_{eq} fall very well on a straight line, indicating close to ideal behavior in the temperature range of 675–800°C. From the linear fit, one obtains $\Delta H^0 = -105$ KJ/mol and $\Delta S^0 = -75.5$ J/(mol K). The negative value of ΔH^0 indicates that the incorporation reaction is exothermic. Thus, an increased temperature will shift the reaction toward the left and increase the number of oxygen vacancies. The negative value of the entropy indicates that the entropy is lowered consistent with removal of gaseous oxygen to the lattice. The values of ΔH^0 and ΔS^0 are compared to values reported by Mizusaki et al.[10,11] and Søgaard et al.[12] in Table I. The values of ΔH^0 and ΔS^0 determined here for a thin film are close to values reported for studies on bulk samples. The equilibrium constant of the oxygen incorporation reaction is neither affected by the film thickness nor possible interactions between film and substrate.
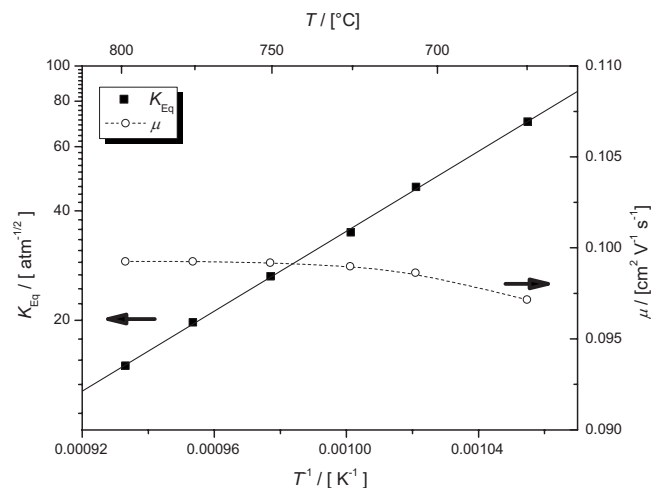
Table I. Comparison between enthalpy and entropy of the surface reaction together with the electron hole mobility.

	Mizusaki et al.[7]	Mizusaki et al.[8]	Søgård et al.[8]	This work
ΔH^0 (kJ/mol)	−100	−109	−90.0	−105
ΔS^0 [J/(mol K)]	−67	−71	−57.7	−75.5
μ [cm²/(V S)]	—	—	0.1–0.2	0.0987
T interval (°C)	600–1200	600–1200	800–1200	650–800
P_{O_2} interval (atm)	10^{-16}–1	10^{-16}–1	10^{-17}–0.21	0.003–1

Table I also shows the values of the apparent electron hole mobility (calculated directly from the measured conductivity, not taking into account the effects of porosities in the film) in comparison to the values obtained by Søgaard et al.[12] for dense bulk samples. Figure 5 also shows the calculated apparent hole mobility (right axis). It is seen that it varies in the range 0.0993 cm² V⁻¹ s⁻¹ at 800°C to 0.0972 cm² V⁻¹ s⁻¹ at 675°C. An average value for hole mobility is 0.0987, which differs from the bulk values reported by Søgaard,[12,13] where the electron hole mobility was observed to increase with the oxygen content from μ = 0.1 cm² V⁻¹ s⁻¹ at δ = 0.16 to μ = 0.2 at δ = 0.06. Patrakeev et al.[5] also measured the electron hole mobility for the system $La_{1-x}Sr_xFeO_{3-\delta}$ (x = 0.2, 0.5, 0.7, 0.9, and 1). It was found that the hole mobility in $La_{0.5}Sr_{0.5}FeO_{3-\delta}$ is higher than for the other Sr contents, it increases linearly with oxygen content, and lies in the range of 0.05–0.25 cm² V⁻¹ s⁻¹.

Taking data from the measurements of Søgaard et al.[12] (conductivity vs P_{O_2}) and fitting them using Eq. 25, one finds a hole mobility that increases from 0.21 cm² V⁻¹ s⁻¹ at 700°C to 0.25 cm² V⁻¹ s⁻¹ at 800°C in the pressure range of 0.001–0.21 atm. The lower apparent hole mobility calculated for the thin film compared to the bulk value is thus not due to the small differences in the applied defect models between this study and the study of Søgaard. It is due to the closed pores in the thin film after heating (as observed in the SEM images in Fig. 3) and is thus an effect of porosity/tortuosity. From the fitted values of K_{eq}, the vacancy concentration (δ) and the thermodynamic factor (Γ_V) at equilibrium can be calculated using Eq. 20 and 24, respectively. δ and Γ_V are plotted as a function of oxygen partial pressure in the temperature range of 650–800°C in Fig. 6 and 7, respectively.

Figure 6 shows that the nonstoichiometry parameter increases with increasing temperature and decreasing oxygen partial pressure.

Figure 5. Reaction equilibrium constant, K_{eq}, as a function of the reciprocal temperature (left axis). Also shown is the electron hole mobility (right axis).
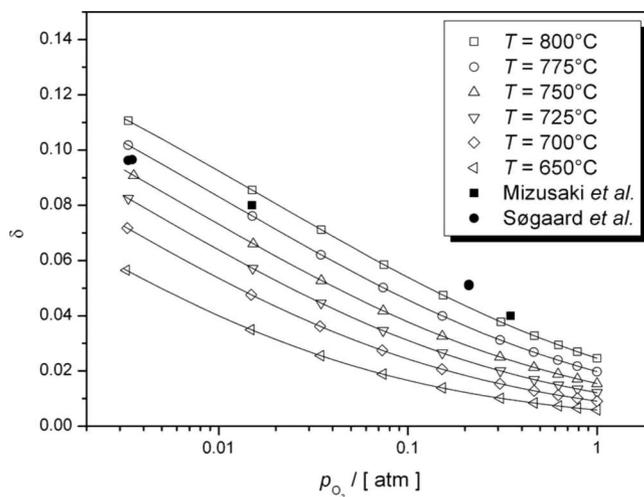

Figure 6. The oxygen nonstoichiometry parameter, δ, as a function of the oxygen partial pressure, P_{O_2}. δ has been calculated on the basis of the values shown in Fig. 5.
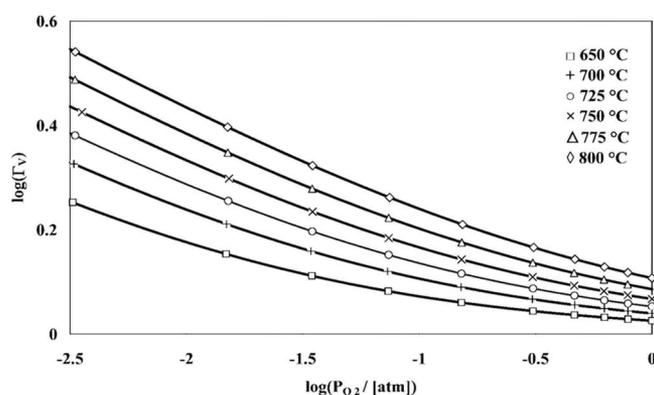
Figure 7. Thermodynamic factor for vacancies, Γ_V, as a function of the oxygen partial pressure, P_{O_2} at different temperatures. Γ_V has been calculated using Eq. 21.

Figure 9. Chemical exchange coefficient, K_{chem}, of LSF64 film as a function of P_{O_2} between 675–800°C.

In Fig. 6, results obtained using thermogravimetry at 800°C by Mizusaki et al.[11] and Søgaard et al.[12] are also shown. Considering the different measurement methods and the difference in data analysis, the agreement between the values of δ obtained in this study and the literature values is rather good.

Conductivity relaxation.— Typical examples of relaxation curves of the electrical conductivity for oxidation steps at 700°C at different oxygen partial pressures together with the respective fitted curves (cf. Eq. 16) are presented in Fig. 8. As evident from Fig. 8, Eq. 16 provides an excellent fit to the experimental data (the measured data and the calculated curves are effectively indistinguishable in the plots). For the relaxation corresponding to the step in P_{O_2} $0.073 \rightarrow 0.151$ atm, a relaxation time of ~ 2000 s was observed, whereas for the relaxation P_{O_2} $0.015 \rightarrow 0.034$ atm, a relaxation time of ~ 3000 s was observed. The time to reach equilibrium thus increases as the oxygen partial pressure decreases. From the fitted curves values of K_{chem} are extracted.

Also, the variation of the chemical exchange coefficient, K_{chem}, with temperature and final oxygen partial pressure was investigated. (For small perturbations, it does not matter if the exchange coefficient is plotted as a function of final or initial P_{O_2}.) The logarithm of K_{chem} obtained from the relaxation curves is plotted as a function of $\log(P_{O_2})$ at different temperatures in Fig. 9. The values of K_{chem} measured here for a 657 nm thick film are very low compared to the values of K_{ex} obtained by ten Elshof et al.[14] and the values k_{Ex} obtained by Søgaard et al.[12] for bulk samples. The slope m
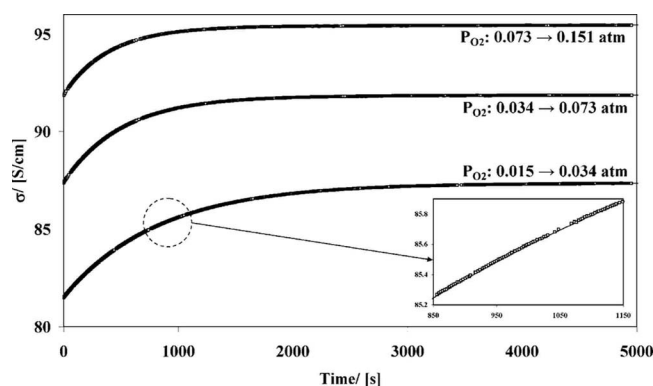

Figure 8. Measured conductivity, σ, as a function of time (circles) for three different stepwise changes in the oxygen partial pressures at 700°C. Also shown is the fitted curve (line) using Eq. 16 for each of the relaxations. The fitted curve is almost superimposed on the measured data.
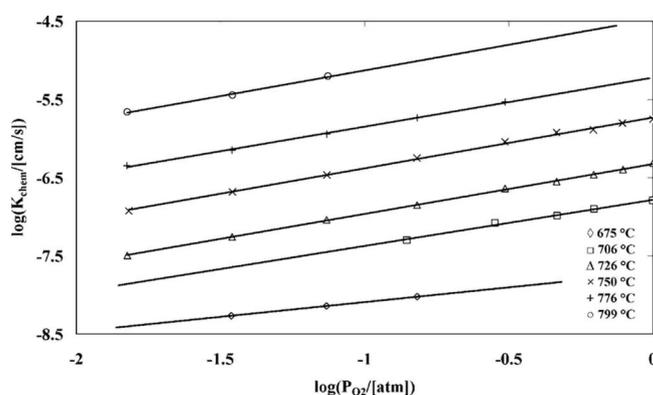
$= d(\log K_{chem})/d(\log P_{O_2})$ increases from 0.43 at 675°C to 0.66 at 799°C. ten Elshof et al.[14] reports $m = 0.75$–0.83 ($K_{ex} \propto P_{O_2}^m$) in the P_{O_2} interval between $10^{-5.5}$ and 0.21 atm and at temperatures between 650 and 950°C. Søgaard et al.[12] obtained $k_{Ex} \propto P_{O_2}^m$ with $0.62 < m < 1.22$ ($700 < T < 1000$°C, $0.004 < P_{O_2} < 0.21$ atm).

Søgaard[13] also measured the chemical surface exchange coefficient on thin film LSF64 deposited on MgO (100) single crystal by PLD. The chemical surface exchange coefficient for the film (570 nm) was found to be significantly lower than that of bulk (e.g., 5.4×10^{-7} cm/s for the film vs 1.2×10^{-5} cm/s for the bulk upon a change in P_{O_2} from 0.006 to 0.011 atm, $T = 700$°C). The corresponding value for K_{chem} in this study was 3.73×10^{-8} cm/s (3 orders of magnitude smaller than the value observed for bulk and 10 times smaller than that found in the LSF thin-film study by Søgaard). The film studied by Søgaard was not heat-treated prior to the relaxation experiments (unlike the one studied here). We have observed (Fig. 2) that the transport properties of the thin film changed on long annealing times due to the change in grain size and film morphology. The film in Søgaard's study has an electrical conductivity by a factor of 4 lower than the film in this study e.g., 20.5 S/cm for Søgaard's[13] film vs 81.5 S/cm for the film in this study, $P_{O_2} = 0.011$ atm $T = 700$°C). Moreover, in the study by Søgaard,[13] the relaxations could not be well fitted with a single exponential function. This, together with the observation of a strongly reduced electronic conductivity in the film, shows that the film studied is structurally unrelaxed. The factor of 10 observed between the determined K_{chem} values between the two studies most likely has its origin in this difference in microstructure.

Sasaki and Maier[30] have measured the chemical exchange coefficient of oxygen at single-crystal yttria-stabilized zirconia surfaces with different orientations. The study shows that K_{chem} depends on surface orientation, and the value of K_{chem} for the single crystal differs from the value for the polycrystalline sample. Sasaki and Maier[30] also investigated the dependence of K_{chem} on annealing time. The experimental measurements show that K_{chem} decreases with increasing annealing time. Chen et al.[31] used the PLD technique for deposition of $La_{0.5}Sr_{0.5}CoO_{3-\delta}$ with 1 μm in thickness on $LaAlO_3$ single crystal. They observed a significant difference in K_{chem} determined from bulk sample and thin film. The observed difference was attributed to a difference in the microstructure and morphology between deposited films and samples made by conventional ceramic processing techniques. Hence, in the above discussed three studies of oxygen exchange kinetics on thin films[13,30,31] deviations from the behavior observed from bulk samples are reported as also observed in this study.

In the calculation of K_{chem}, the solid-gas interface area is assumed to be the geometric area of the film ($A_s/A_g \sim 1$). If the specific pore surface area of the porous film (Fig. 3) with porosity ε is
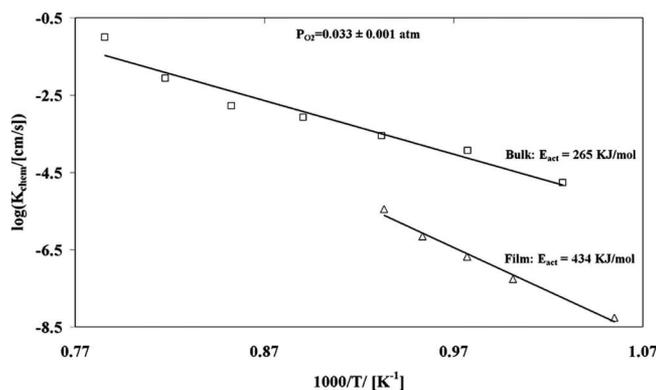
Figure 10. Arrhenius-type plot of the chemical exchange coefficient, K_{chem}, of LSF64 film and values for a bulk sample from Søgaard et al.[18]

Figure 12. Comparison of k_O calculated in this study and k_O measured by ten Elshof et al.[14] for a bulk sample at 726°C.

given by S_V (in centimeters squared per cubic centimeter), Eq. 1 must be corrected and the rate of oxygen incorporation is given by[32]

$$S_V K_{chem}(\delta - \delta_\infty) = -(1 - \varepsilon)\frac{d\delta}{dt} \qquad [54]$$

Thus, the calculated value of K_{chem} is affected by the specific surface area and porosity, which depends on the structure and morphology of the film. It is, however, unlikely that it is the correction for porosity and surface area, which is the reason for the observed discrepancy between the K_{chem} of the film and the bulk, as it would require differences in A_s/A_g between bulk and thin film of a factor of 1000. Considering the observed microstructure of the relaxed film, this does not seem likely. The values of the chemical exchange coefficient for the LSF64 film (012 oriented) at $P_{O_2} = 0.033 \pm 0.001$ atm are compared to data for bulk samples[12,13] in Fig. 10. The activation energy is found to be 434 kJ/mol for the thin film, whereas 265 kJ/mol is reported for the bulk sample, which could suggest different reaction mechanisms.

The logarithm of the vacancy surface exchange coefficient, k_V (cf., Eq. 34), obtained from the fitted data, is calculated and plotted as a function of $\log(P_{O_2})$ at different temperatures in Fig. 11. The values for the thermodynamic factor Γ_V from Fig. 7 were used to calculate k_V. Figure 11 shows that k_V increases monotonically with increasing P_{O_2}. The slope increases from 0.51 at 675°C to 0.85 at 799°C. The size of the symbols in Fig. 11 shows the maximum error bars in the exchange coefficient. The error on the k_V is very small ($1\% \le \Delta k_V/k_V \le 5\%$, the error is calculated with two σ confidence limits). The error increases with increasing oxygen partial pressure from 1 to 5%. In the region $T > 800°C$, the relaxation time is very
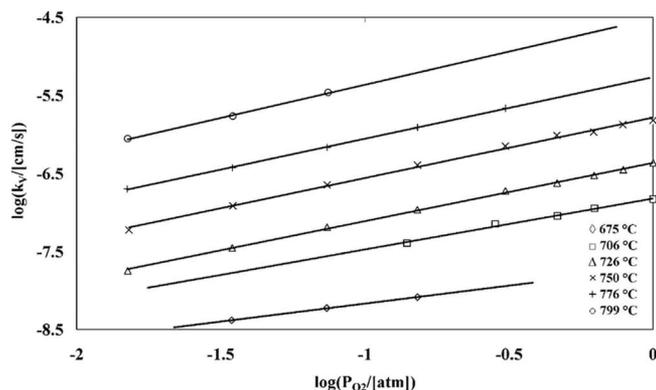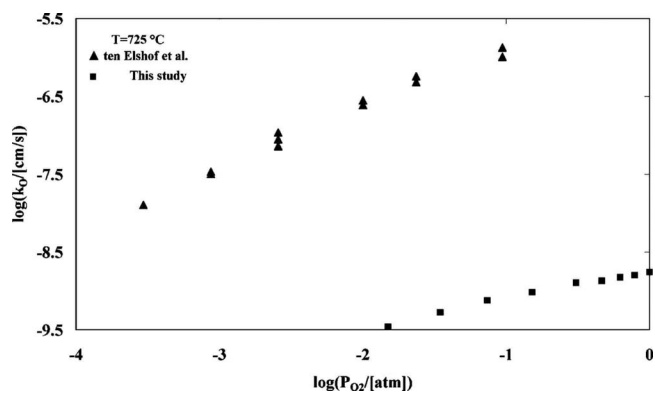
short and a precise evaluation of K_{chem} is difficult (because the relaxation time is comparable to the time needed for changing the gas in the reactor).

The oxygen surface exchange coefficient, k_O, calculated from k_V and $\delta_\infty [k_V\delta = k_O(3 - \delta)]$ obtained for the thin film are compared to the values k_O reported by ten Elshof et al.[14] at 725°C in Fig. 12. As also discussed in the comparison of the K_{chem} values, the values of k_O for the thin film are much smaller than the values reported for the bulk samples. The explanation(s) for the slower exchange kinetics on thin films is, at present, not known to us and will be addressed in future work. It should be noted that other thin-film studies have reported on the exchange properties being different from values observed on bulk samples.[13,31,30] However, we speculate that it could originate from (*i*) orientation effects: The thin films investigated in this study were oriented contrary to a bulk sample, where many crystal orientations are present at the surface. It is possible that the effect of the lower surface exchange kinetics is simply a matter of slower exchange kinetics on the facet that is exposed on the thin film in this study. (*ii*) Impurities: It is well known from SOFC studies that impurities such as SiO_2, Na_2O segregate to the surface forming glassy phases.[33] It is possible that the kinetics on the thin films studied here are somehow more strongly impeded by impurities than is the case for bulk samples.

Also when comparing the P_{O_2} dependence of the reaction rate on the thin film with reports based on bulk samples in terms of the k_O values, smaller exponents are found for the thin film than for the bulk. We found the slope of $\log(k_O)$ vs $\log(P_{O_2})$ to be between 0.22 and 0.61. ten Elshof et al.[14] report a slope between 0.65 and 0.84 and Søgaard et al.[12,13] report values of n that varies from 0.55 at 800°C to 1.20 at 1000°C for bulk samples. At 800°C, where the results can be compared, a reaction order with respect to oxygen of 0.55 is reported by Søgaard, which is close to that obtained by ten Elshof et al. and fairly close to the value of 0.61 found here. Preis et al.[34] have studied the oxygen exchange kinetics of polycrystalline $La_{0.4}Sr_{0.6}FeO_{3-\delta}$ by both relaxation and carrier gas coulometric techniques. They report that k_{exc} (equivalent to K_{chem}) is proportional to $P_{O_2}^n$ with n between 0.66 at 900°C to 0.81 at 700°C.

Evaluation of the possible reaction mechanisms.— The mechanism of the oxygen incorporation reaction can be investigated by measurement of the vacancy surface exchange coefficient, k_V, and the relation to the oxygen partial pressure and defects concentration for the simple situation close to equilibrium. The calculated k_V values are now compared to models for the different possible mechanisms divided into specific elementary steps, including adsorption, dissociation, and incorporation, which were presented in the theory section and Appendix C. According to the summary of the different mechanisms in Appendix C there are a number of different possibilities for the reaction mechanism that gives rise to slope of log
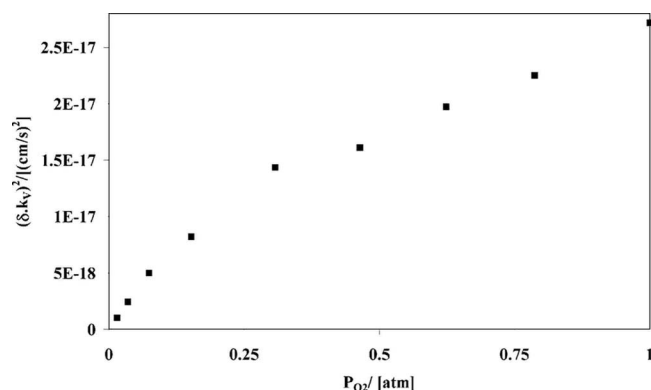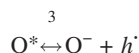

Figure 11. Surface exchange coefficient, k_V, of the LSF64 film as a function of P_{O_2} between 675–800°C.

Figure 13. $(\delta \cdot k_V)^2$ as a function of P_{O_2} at a temperature 726°C.

Figure 14. k_V/δ as a function of P_{O_2} at different temperature for LSF64 thin film. The inset shows a magnified part of the plot, clearly illustrating the linearity.

(k_V) vs $\log(P_{O_2})$ in the interval from 0.5 to 1 (see Fig. 11). In the following, we shall investigate all of the suggested reaction schemes that have an exponent in this interval.

In the reaction schemes 3–7 in Appendix C the first step is the splitting of oxygen to either ionic species (O^- or O^{-2}) or adsorbed O^* on the surface. This step yields a surface-exchange coefficient $k_V \propto P_{O_2}^{1/2}\delta_\infty^{-1}$ with a slope between $1/2 < n < 1$ ($k_V \propto P_{O_2}^n$). These models thus predict a linear relationship between $(\delta k_V)^2$ vs P_{O_2} at any temperature. Our experimental data do not show this linearity and are off from the model at all temperatures. For the sake of illustration, Fig. 13 shows $(\delta k_V)^2$ vs P_{O_2} at 726°C. The reaction schemes 3–7 can thus be ruled out. With step 3 in mechanisms 14 and 15, namely,

$$O^* \overset{3}{\leftrightarrow} O^- + h^{\cdot}$$

step 2 in mechanisms 17 and with step 1 and 2 in mechanism 16 as the RDSs, the same P_{O_2} and δ dependence of the surface exchange coefficient $k_V \propto P_{O_2}^{1/2}\delta_\infty^{-1}$ would be observed. For the same reason, these mechanisms can also be ruled out.

In the reaction schemes 10, 11, and 18 in Appendix C, the first step is adsorption of an oxygen molecule on a vacancy, $O_2 + V_O^{\cdot\cdot} \leftrightarrow (O_2 \cdots V_O^{\cdot\cdot})$. The second step is either splitting of $(O_2 \cdots V_O^{\cdot\cdot})$ to $(O \cdots V_O^{\cdot\cdot})$ (in the reaction scheme 10) or formation of $(O_2 \cdots V_O^{\cdot\cdot} \cdots O_2)$ (in reaction scheme 11). These steps as the RDS yield a surface-exchange coefficient $k_V \propto P_{O_2}\delta_\infty$ with a slope between $1/2 < n < 1$ ($k_V \propto P_{O_2}^n$). The expression for k_V thus predicts a linear relationship between k_V/δ vs P_{O_2} at any temperature. This is indeed observed as can be seen in Fig. 14 at temperatures between 675–799°C, and the results (Fig. 14) thus indicate that step 2 in the reaction schemes 10 and 11 and 18 in Appendix C could be RDS. With step 3 in mechanism 11 as the RDS, the same P_{O_2} and δ dependence of the surface exchange coefficient would be observed why this step could also be the RDS. Hence, only a subset of five out of the analyzed schemes (see Appendix C) predict the here-observed P_{O_2} dependence. For instance, the simplest possible scheme of the process, assuming that it is a one-step process between an oxygen molecule and two vacancies (scheme 1) predicts a wrong P_{O_2} dependence. Many two-step mechanisms have been suggested in literature[19-21,25,27,35,36] for similar materials, where the first step is either dissociative adsorption on two vacancies (scheme 2),[20] dissociative adsorption on some surface site (scheme 3)[21,27] or a dissociative adsorption involving a charge transfer (schemes 4,5).[21,25,27,35] None of these predict the here-observed P_{O_2} dependence. The only two-step processes found to be consistent with the observations are schemes 18 and 19
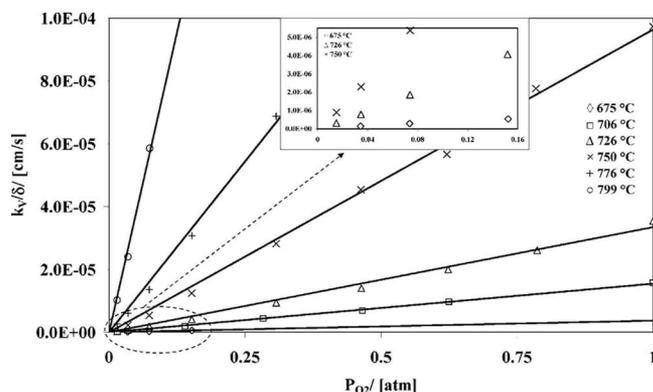
1.
$$O_2 + V_O^{\cdot} \overset{1}{\leftrightarrow} (O_2 \cdots V_O^{\cdot\cdot})$$
$$(O_2 \cdots V_O^{\cdot\cdot}) + V_O^{\cdot\cdot} \overset{2}{\leftrightarrow} 2O_O^X + 4h^{\cdot}$$

where step 2 is RDS and

2.
$$O_2 + (V_O^{\cdot\cdot} \cdots V_O^{\cdot\cdot}) \overset{1}{\leftrightarrow} 2(O \cdots V_O^{\cdot\cdot})$$
$$(O \cdots V_O^{\cdot\cdot}) \overset{2}{\leftrightarrow} O_O^X + 2h^{\cdot}$$
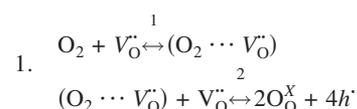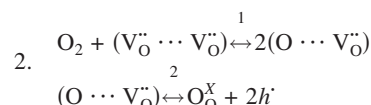
with the first step as rate determining.

Considering more complex schemes breaking the reaction into three or more steps, the following two possibilities (mechanisms 10 and 11) are consistent with the observations

3.
$$O_2 + V_O^{\cdot} \overset{1}{\leftrightarrow} (O_2 \cdots V_O^{\cdot\cdot})$$
$$(O_2 \cdots V_O^{\cdot\cdot}) + V_O^{\cdot\cdot} \overset{2}{\leftrightarrow} 2(O \cdots V_O^{\cdot\cdot})$$
$$(O \cdots V_O^{\cdot\cdot}) \overset{3}{\leftrightarrow} O_O^X + 2h^{\cdot}$$

with step 2 as RDS or

4.
$$O_2 + V_O^{\cdot} \overset{1}{\leftrightarrow} (O_2 \cdots V_O^{\cdot\cdot})$$
$$(O_2 \cdots V_O^{\cdot\cdot}) + V_O^{\cdot\cdot} \overset{2}{\leftrightarrow} (V_O^{\cdot\cdot} \cdots O_2 \cdots V_O^{\cdot\cdot})$$
$$(V_O^{\cdot\cdot} \cdots O_2 \cdots V_O^{\cdot\cdot}) \overset{3}{\leftrightarrow} 2(O \cdots V_O^{\cdot\cdot})$$
$$(O \cdots V_O^{\cdot\cdot}) \overset{4}{\leftrightarrow} O_O^X + 2h^{\cdot}$$
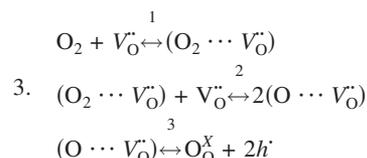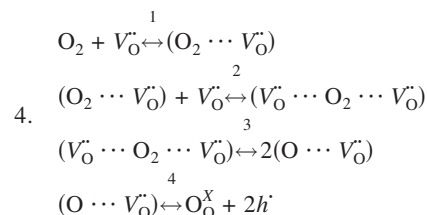
with either steps 2 or 3 as the RDS.

Hence, for this material (in the considered P_{O_2} and temperature range) we can rule out the three-step mechanisms suggested for the oxygen incorporation reaction on various similar perovskite materials in Ref. 21, 24, 25, and 34-38.

The analyses above indicates that the first step of the oxygen-exchange process is adsorption of molecular oxygen on a vacancy that reacts as an adsorb site according to

$$O_2 + V_O^{\cdot} \overset{1}{\leftrightarrow} (O_2 \cdots V_O^{\cdot\cdot})$$
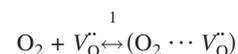
This step takes place very fast such that one can assume the reactants and intermediate product are in equilibrium. Under this assumption the concentration of the adsorbate can be written
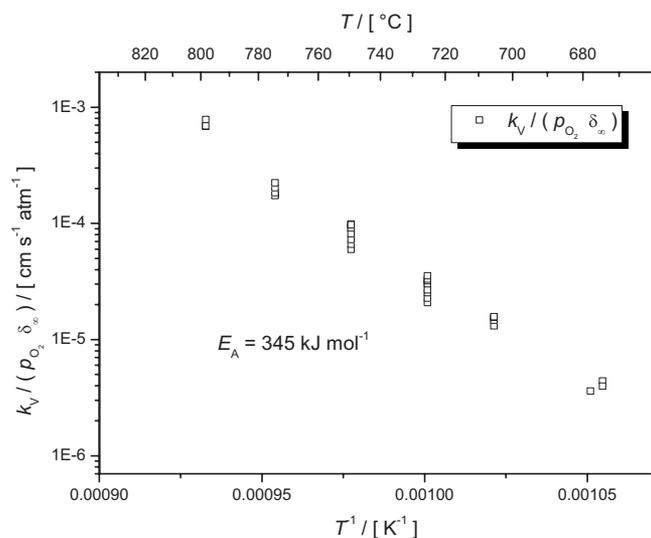
Figure 15. Arrhenius-type plot of K ($k_V = LKP_{O_2}\delta_\infty$) for LSF64 thin film.

$$[O_2 \cdots V_O^{\cdot\cdot}] = K_1^{eq}P_{O_2}\delta \qquad [55]$$

The rate of the incorporation reaction is directly dependent on the concentration of the above species with the following expression for the surface exchange coefficient

$$\frac{k_V}{L} = KP_{O_2}\delta_\infty \text{ or } \frac{k_O}{L} = KP_{O_2}\frac{\delta_\infty^2}{3 - \delta_\infty} \qquad [56]$$

By differentiation of Eq. 56, one can show that

$$\frac{d\log k_V}{d\log P_{O_2}} = 1 - \frac{1}{2\Gamma_V} \qquad [57]$$

Equation 57 shows that the slope of $\log(k_V)$ vs $\log(P_{O_2})$ lies in the interval 0.5–1. This slope depends on the thermodynamic factor, which is a function of temperature and oxygen partial pressure. Therefore depending on the range of P_{O_2}, a wide range of values for the slope (between 0.5 and 1) can be reported for the same material.

The temperature dependence of K in Eq. 56 can be calculated by fitting the experimental data for $k_v/(pO_2 \cdot \delta)$ vs the reciprocal absolute temperature. This is illustrated in Fig. 15, where $k_v/(pO_2 \cdot \delta)$ is plotted vs $1/T$. A fair linearity is observed in the plot, showing that $k_v/(pO_2 \cdot 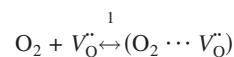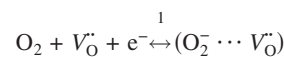\delta)$ describes a thermally activated process as expected, it being a product of a reaction rate constant and an equilibrium constant (Appendix C, schemes 10, 11, 18, and 19). The deduced activation energy is 345 kJ/mol.

Equation 56 is not consistent with Eq. 26 in the work of ten Elshof et al.[14] who measured k_O on bulk LSF64 at temperatures between 650 and 950°C and pressure between $10^{-5.5}$ and 1 atm. They observed a linear relationship between k_O/P_{O_2} and δ and concluded that both reactions, $O_2 + V_O^{\cdot\cdot} \leftrightarrow (O_2 \cdots V_O^{\cdot\cdot})$ and $O_2 + V_O^{\cdot\cdot} + e^- \leftrightarrow (O_2^- \cdots V_O^{\cdot\cdot})$ could be RDSs. In bulk samples, the uncertainty in measurements of the exchange coefficient (introduced by the simultaneous determination of k and D), in general, makes it more difficult to determine reaction orders accurately. Measurements on thin film are more accurate; however, from the large discrepancy between the magnitude of k_O and its temperature dependence observed between this study on thin film and bulk samples, one cannot be sure that the reaction occurs via the same mechanism. For the thin film, the absorption of oxygen molecules on vacancies is not the RDS. Our measurements show that $k_V \propto P_{O_2}\delta_\infty$ or $k_O \propto P_{O_2}\delta_\infty^2$. As discussed above in analyzing the different possible mechanisms, this points to the splitting of O_2 adsorbed on a vacancy to be RDS rather than
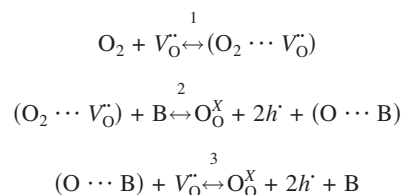
$$O_2 + V_O^{\cdot\cdot} \overset{1}{\leftrightarrow} (O_2 \cdots V_O^{\cdot\cdot})$$

or

$$O_2 + V_O^{\cdot\cdot} + e^- \overset{1}{\leftrightarrow} (O_2^- \cdots V_O^{\cdot\cdot})$$

as was suggested to be the RDS on bulk LSF64 samples.[14]

There are some common features to the five possible reaction schemes identified above (the scheme marked four counts twice because either step 2 or 3 could be the RDS). Common to four of them (1, 2, 3, and 4 with step 3 as the RDS) is that it is the step involving the splitting of the molecule that is rate determining. [In the last case, it is the formation of a double-coordinated adsorbed oxygen molecule (4 with 2 as the RDS)]. In four of the cases, the first step is adsorption of an oxygen molecule on a vacancy, which occurs fast. In the last case, the adsorption is dissociative (2). It involves two vacancies and becomes the RDS.

The expression for k_V, Eq. 56, together with the above-identified mechanisms indicates that to obtain high surface exchange rates one needs many vacancies with high mobility. This is in good accord with the point made by Kilner et al.[39] and DeSouza and Kilner[40] that the parameters, oxygen surface exchange coefficient, k_O, and oxygen diffusion coefficient, D_O, are strongly correlated when considered over a very broad class of materials. Increasing the oxygen vacancy concentration can be achieved by changing the material composition (e.g., by increasing the amount of divalent dopant or by substitution on the iron site with other elements such as Co).

It should be noted that in the analysis or the reaction mechanism (Appendix C) the treatment is limited to the case where one can assume one step to be rate determining. This is not necessarily the case (i.e., more of the analyzed mechanisms could well give the observed reaction order if one relaxes the requirement of a single RDS). For instance, the scheme below (22 in Appendix C)

$$O_2 + V_O^{\cdot\cdot} \overset{1}{\leftrightarrow} (O_2 \cdots V_O^{\cdot\cdot})$$

$$(O_2 \cdots V_O^{\cdot\cdot}) + B \overset{2}{\leftrightarrow} O_O^X + 2h^\cdot + (O \cdots B)$$

$$(O \cdots B) + V_O^{\cdot\cdot} \overset{3}{\leftrightarrow} O_O^X + 2h^\cdot + B$$

involving after the adsorption an incorporation of one atom and the establishment of an adsorbed atomic species at some other site on the surface (illustrated here as being above a B-site) could well be shown to be consistent with the observations if one abandons the assumption of a single RDS [i.e., it is possible to find a number of rates (and equilibrium constants) all assumed to show an Arrhenius-type temperature dependence that would make the model account for the observed exchange rates over the investigated P_{O_2} and temperature interval].

Conclusion

A $(La_{0.6}Sr_{0.4})_{0.99}FeO_{3-\delta}$ (LSF64) thin film was deposited on a MgO (100) single crystal. The thickness of the film was 657 nm. The electrical properties were measured by electrical conductivity relaxation in the temperature range of 650–800°C and over the P_{O_2} range of 0.001–1 atm. It was found that thin film and bulk material have the same oxygen stoichiometry at a given temperature and oxygen partial pressure. The equilibrium constant (K_{eq}) of incorporation reaction follows a Van't Hoff relation with reaction entropy, $\Delta H^0 = -105$ kJ/mol and reaction enthalpy, $\Delta S^0 = -75.5$ J/(mol K) similar to values determined by others for the bulk material. A simplified defect model was formulated for the LSF considering electron holes and oxygen vacancies as the only defects. (The model does not describe how the holes are distributed over the lattice and is thus a simplification relative to the normally applied "chemical picture," where the holes are assumed to be associated with Fe). The model was found to account well for the observed stoichiometry and conductivity as well as their P_{O_2} and temperature dependence. It

allows closed-form expressions for the defect concentrations, and the thermodynamic properties such as equilibrium constant, electrical conductivity, and defect concentrations can all be expressed as a function of the thermodynamic factor (Γ_V), given by $\Gamma_V = \sqrt{1 + 24x/(K_{eq}P_{O_2}^{1/2})}$.

The ECR technique performed on thin LSF64 film appears to be a good tool for characterizing the oxygen surface reaction. Relaxation curves showed a good fit to a simple exponential decay. The values of K_{chem} measured here for a 657 nm thick film were significantly lower than the values reported for bulk samples. The values of k_V, calculated from K_{chem} and Γ_V show a slope (log k_V vs log P_{O_2}) between 0.51 and 0.85. It is found that k_V is proportional to the product of oxygen partial pressure and the vacancy concentration ($k_V \propto P_{O_2}\delta_\infty$ or $k_O \propto P_{O_2}\delta_\infty^2$). Because the vacancy concentration has a negative exponent in oxygen partial pressure, the overall P_{O_2} dependency of k_V has order between 0.5 and 1 (the overall P_{O_2} dependency of k_O has order between 0 and 1).

A number of possible surface reaction mechanisms were analyzed under the assumption of a single step being rate determining. Out of the 22 analyzed models, only 4 gave reaction orders consistent with the observations. It is not possible from these experiments only to conclude by which of these schemes the reaction occurred. There are common features between these possibilities, as follows:

1. It is the step involving the splitting of molecular oxygen that is rate determining (except in one case).

2. In all cases, the first step involves adsorption of molecular oxygen on an oxygen vacancy.
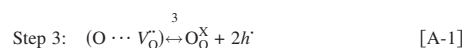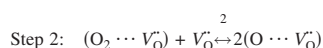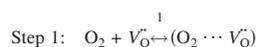
Acknowledgments

Appendix A

The overall oxygen exchange reaction can be divided into the following elementary steps

$$\text{Step 1:} \quad O_2 + V_O^{\cdot\cdot} \overset{1}{\leftrightarrow} (O_2 \cdots V_O^{\cdot\cdot})$$

$$\text{Step 2:} \quad (O_2 \cdots V_O^{\cdot\cdot}) + V_O^{\cdot\cdot} \overset{2}{\leftrightarrow} 2(O \cdots V_O^{\cdot\cdot})$$

$$\text{Step 3:} \quad (O \cdots V_O^{\cdot\cdot}) \overset{3}{\leftrightarrow} O_O^X + 2h^{\cdot} \qquad [\text{A-1}]$$

According to the above mechanism, the rate of the elementary reactions is governed by

$$r_1 = k_1 P_{O_2}\delta - k_{-1}Y$$

$$r_2 = k_2 Y\delta - k_{-2}Z^2$$

$$r_3 = k_3 Z - 3k_{-3}(x - 2\delta)^2 \qquad [\text{A-2}]$$

where k_i and k_{-i} are the rate constants of forward and backward reactions of the related step, respectively, that depends only on temperature.

The net rate of the overall surface reaction corresponding to the oxygen incorporation is related to r_1, r_2, and r_3

$$r = 2r_1 = 2r_2 = r_3 \qquad [\text{A-3}]$$

Y and Z denote the concentration of the surface intermediates defined as follows

$$Y = [O_2 \cdots V_O^{\cdot\cdot}]$$

$$Z = [O \cdots V_O^{\cdot\cdot}] \qquad [\text{A-4}]$$

By applying the quasi-steady-state conditions, the following equations must be solved for Y and Z in terms of P_{O_2} and δ

$$\frac{dY}{dt} = 0 \Rightarrow r_1 - r_2 = 0$$

$$\frac{dZ}{dt} = 0 \Rightarrow 2r_2 - r_3 = 0 \qquad [\text{A-5}]$$

By solving the system of Eq. A-5, the concentration of intermediate species Z can be calculated as the positive root of the following quadratic equation

$$Z^2 + 2\Delta \cdot Z - \left[\left(\frac{K_{eq}}{K_3^{eq}}\right)^2 P_{O_2}\delta^2 + \frac{6\Delta}{K_3^{eq}}(x - 2\delta)^2\right] = 0 \qquad [\text{A-6}]$$

where Δ is defined as a help factor by

$$\Delta = \frac{k_3}{4k_{-1}k_{-2}}(k_{-1} + k_2\delta) \qquad [\text{A-7}]$$

The solution for Z becomes

$$Z = \sqrt{D} - \Delta \qquad [\text{A-8}]$$

where D is the discriminant of the quadratic equation, which can be expressed by

$$D = \Delta^2 + \left(\frac{K_{eq}}{K_3^{eq}}\right)^2 P_{O_2}\delta^2 + \frac{6\Delta}{K_3^{eq}}(x - 2\delta)^2 \qquad [\text{A-9}]$$

At the equilibrium, one can calculate the square root of D by using Eq. 19 at the equilibrium

$$\sqrt{D_\infty} = \frac{K_{eq}}{K_3^{eq}}P_{O_2}^{1/2}\delta_\infty + \Delta_\infty \qquad [\text{A-10}]$$

The values of different quantities compared with the values at equilibrium can be obtained as follows

$$\frac{\Delta - \Delta_\infty}{\delta - \delta_\infty} = \frac{k_3}{4k_{-1}k_{-2}}k_2$$

$$\frac{\Delta\delta - \Delta_\infty\delta_\infty}{\delta - \delta_\infty} = \frac{k_3}{4k_{-1}k_{-2}}(\Delta + \Delta_\infty - k_{-1})$$

$$\frac{\Delta\delta^2 - \Delta_\infty\delta_\infty^2}{\delta - \delta_\infty} = \frac{k_3}{4k_{-1}k_{-2}}(\delta\Delta + \delta_\infty\Delta_\infty + k_2\delta\delta_\infty)$$

$$\frac{\Delta(x - 2\delta)^2 - \Delta_\infty(x - 2\delta_\infty)^2}{\delta - \delta_\infty} = \frac{k_3}{4k_{-1}k_{-2}}k_2(x - 2\delta)(x - 2\delta_\infty)$$
$$- 2[\Delta(x - 2\delta) + \Delta_\infty(x - 2\delta_\infty)] \qquad [\text{A-11}]$$

and the corresponding value for D is

$$\frac{D - D_\infty}{\delta - \delta_\infty} = \frac{k_3}{4k_{-1}k_{-2}}k_2(\Delta + \Delta_\infty) + \left(\frac{K_{eq}}{K_3^{eq}}\right)^2 P_{O_2}(\delta + \delta_\infty)$$
$$+ \frac{6}{K_3^{eq}}\left\{\frac{k_3}{4k_{-1}k_{-2}}k_2(x - 2\delta)(x - 2\delta_\infty) - 2[\Delta(x - 2\delta) + \Delta_\infty(x - 2\delta_\infty)]\right\}$$
$$[\text{A-12}]$$

The overall reaction rate can be expressed as follows

$$r = k_3\left(Z - \frac{3(x - 2\delta)^2}{K_3^{eq}}\right) \qquad [\text{A-13}]$$

In Eq. A-13, it is assumed that the oxygen nonstoichiometry, δ remains small and thus the fraction of lattice oxygen, O_O^X remains constant, equal to 3.

At equilibrium (for $t \to \infty$), the reaction rate approaches zero and we may write

$$0 = k_3\left(Z_\infty - \frac{3(x - 2\delta_\infty)^2}{K_3^{eq}}\right) \qquad [\text{A-14}]$$

By subtracting Eq. A-14 from Eq. A-13, we obtain

$$r = k_3\left(Z - Z_\infty - \frac{3(x - 2\delta)^2}{K_3^{eq}} + \frac{3(x - 2\delta_\infty)^2}{K_3^{eq}}\right) \qquad [\text{A-15}]$$

By using the solution for Z, the following equation is obtained for the reaction rate

$$r = k_3\left((\sqrt{D} - \sqrt{D_\infty}) - (\Delta - \Delta_\infty) - \frac{3(x - 2\delta)^2}{K_3^{eq}} + \frac{3(x - 2\delta_\infty)^2}{K_3^{eq}}\right) \qquad [\text{A-16}]$$

Rearrangement of Eq. A-16 gives

$$r = k_3\left(\frac{D - D_\infty}{\sqrt{D} + \sqrt{D_\infty}} - (\Delta - \Delta_\infty) - \frac{3(x - 2\delta)^2}{K_3^{eq}} + \frac{3(x - 2\delta_\infty)^2}{K_3^{eq}}\right) \qquad [\text{A-17}]$$

By using the values from Eq. A-11 and A-12, one gets

$$r = k_3 \left[\frac{1}{\sqrt{D} + \sqrt{D_\infty}} \left(\frac{k_3}{4k_{-1}k_{-2}} k_2(\Delta + \Delta_\infty) + \left(\frac{K_{eq}}{K_3^{eq}} \right)^2 P_{O_2}(\delta + \delta_\infty) \right. \right.$$
$$\left. + \frac{6}{K_3^{eq}} \left\{ \frac{k_3}{4k_{-1}k_{-2}} k_2(x - 2\delta)(x - 2\delta_\infty) - 2[\Delta(x - 2\delta) + \Delta_\infty(x - 2\delta_\infty)] \right\} \right)$$
$$\left. - \frac{k_3}{4k_{-1}k_{-2}} k_2 + \frac{12}{K_3^{eq}}(x - \delta - \delta_\infty) \right] (\delta - \delta_\infty) \qquad \text{[A-18]}$$

The consumption rate of the vacancies is related to the net reaction rate by

$$-\frac{d\delta}{dt} = r \qquad \text{[A-19]}$$

Inserting Eq. A-18 into Eq. A-19 and use the definition of K_{chem} from Eq. 2, the following expression can be obtained

$$\frac{K_{chem}}{L} = k_3 \left[\frac{1}{\sqrt{D} + \sqrt{D_\infty}} \left(\frac{k_3}{4k_{-1}k_{-2}} k_2(\Delta + \Delta_\infty) + \left(\frac{K_{eq}}{K_3^{eq}} \right)^2 P_{O_2}(\delta + \delta_\infty) \right. \right.$$
$$\left. + \frac{6}{K_3^{eq}} \left\{ \frac{k_3}{4k_{-1}k_{-2}} k_2(x - 2\delta)(x - 2\delta_\infty) - 2[\Delta(x - 2\delta) + \Delta_\infty(x - 2\delta_\infty)] \right\} \right)$$
$$\left. - \frac{k_3}{4k_{-1}k_{-2}} k_2 + \frac{12}{K_3^{eq}}(x - \delta - \delta_\infty) \right] \qquad \text{[A-20]}$$

The expression for the vacancy exchange coefficient is a complex function of both the values at equilibrium and the values in the transition state. To simplify Eq. A-20, we must make some assumptions. If in relaxation experiment the departure from the equilibrium is small (small perturbation), then one can assume that $\delta \approx \delta_\infty$ and Eq. A-20 can be reduced to

$$\frac{K_{chem}}{L} = k_3 \left\{ \frac{1}{2\sqrt{D_\infty}} \left(\frac{k_3}{4k_{-1}k_{-2}} 2k_2\Delta_\infty + 2 \left(\frac{K_{eq}}{K_3^{eq}} \right)^2 P_{O_2}\delta_\infty + \frac{6}{K_3^{eq}} \left\{ \frac{k_3}{4k_{-1}k_{-2}} k_2(x - 2\delta_\infty)^2 \right. \right. \right.$$
$$\left. \left. - 4\Delta_\infty(x - 2\delta_\infty) \right\} \right) - \frac{k_3}{4k_{-1}k_{-2}} k_2 + \frac{12}{K_3^{eq}}(x - 2\delta_\infty) \right\} \qquad \text{[A-21]}$$

By using the condition at equilibrium, namely, Eq. 19, and applying Eq. A-10, it can be obtained

$$\frac{K_{chem}}{L} = \frac{k_3}{\sqrt{D_\infty}} \left(\frac{K_{eq}}{K_3^{eq}} \right)^2 P_{O_2}\delta_\infty\Gamma_V \qquad \text{[A-22]}$$

Equation A-22 suggests that in the case of small perturbation the K_{chem} is directly proportional with oxygen partial pressure, vacancy concentration, and the thermodynamic factor for vacancies. By inserting the expression for $\sqrt{D_\infty}$, the following is obtained

$$\frac{K_{chem}}{L} = \frac{k_3}{\left(\frac{K_{eq}}{K_3^{eq}} \right) P_{O_2}^{1/2}\delta_\infty + \Delta_\infty} \left(\frac{K_{eq}}{K_3^{eq}} \right)^2 P_{O_2}\delta_\infty\Gamma_V \qquad \text{[A-23]}$$

Inserting the expression for Δ_∞ and rearranging leads to

$$\frac{K_{chem}}{L} = \frac{P_{O_2}\delta_\infty\Gamma_V}{\frac{1}{k_{-3}K_{eq}} P_{O_2}^{1/2}\delta_\infty + \frac{1}{4k_1}\delta_\infty + \frac{1}{4k_2 K_1^{eq}}} \qquad \text{[A-24]}$$

Appendix B

In a situation where the departure from equilibrium is not small, the linear model is not valid and one may investigate the effect of the departure from equilibrium on the kinetics by calculation of the corresponding error, Δ. This can easily be done by varying the ratio of the initial P_{O_2} and final P_{O_2} by using Eq. 29
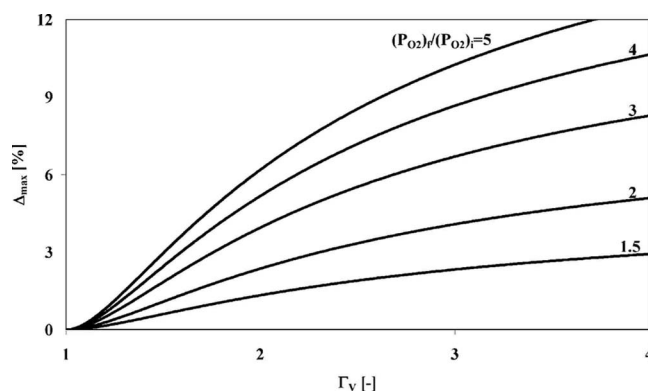

Figure B-1. Maximum displacement from equilibrium as a function of thermodynamic factor at different step change ratios in P_{O_2}. Subscripts f and i indicate final and initial states, respectively

$$\Delta = \frac{\Delta\delta}{\delta_\infty} \frac{(\Gamma_V - 1)^2}{4\Gamma_V} \qquad \text{[B-1]}$$

where $\Delta\delta = \delta - \delta_\infty$ and $\Delta\delta/\delta_\infty$ indicate the absolute departure and relative departure from the equilibrium, respectively. Equation B-1 shows that the departure from equilibrium (Δ) depends not only on the step change in δ but also on the thermodynamic factor.

The maximum error can be calculated if the time dependence δ is replaced by the initial vacancy concentration, δ_0 as follows

$$\Delta_{max} = \frac{\delta_0 - \delta_\infty}{\delta_\infty} \frac{(\Gamma_V - 1)^2}{4\Gamma_V} \qquad \text{[B-2]}$$

Because the vacancy concentration at equilibrium depends on oxygen partial pressure according to $\delta \propto P_{O_2}^{-(1/2\Gamma_V)}$, the P_{O_2} dependency of error has the following expression

$$\Delta_{max} = \left[\left(\frac{(P_{O_2})_f}{(P_{O_2})_i} \right)^{1/2\Gamma_V} - 1 \right] \frac{(\Gamma_V - 1)^2}{4\Gamma_V} \qquad \text{[B-3]}$$

where $(P_{O_2})_f$ and $(P_{O_2})_i$ are the oxygen partial pressures in the final and initial states.

To investigate the effect of the departure from the equilibrium on the surface exchange coefficient k_V, Fig. B-1 illustrates the variation of error as a function of thermodynamic factor for different P_{O_2} ratios. Figure B-1 shows that the error increases with increasing the thermodynamic factor Γ_V, but in all cases the error is <10% if the P_{O_2} step change, namely $(P_{O_2})_f/(P_{O_2})_i$ is <4. The value of Γ_V (depending on temperature and P_{O_2}) in this study lies in the range from 1 to 3.5. For a step change $(P_{O_2})_f/(P_{O_2})_i = 2$ or less, the error does not exceed 5%.

As mentioned above, the thermodynamic factor depends on both oxygen partial pressure and temperature; therefore, the error increases with increasing temperature or decreasing oxygen partial pressure. One can show that as $\Gamma_V \to \infty$, the function $\Delta_{max} \to \text{Ln}[(P_{O_2})_f/(P_{O_2})_i]/8$. The following table shows the asymptotic values for Δ_{max} as a function of P_{O_2} ratio

$(P_{O_2})_f/(P_{O_2})_i$	1.5	2	3	4	5	10
Δ_{max} (%) at $\gamma_{V\to\infty}$	5.07	8.66	13.7	17.3	20.1	28.8

Appendix C

Mechanism	Reaction mechanism	k_V/L (s^{-1})	k_V order in P_{O_2}
1	$(1/2)O_2 + V_O^{\bullet\bullet} \leftrightarrow O_O^X + 2h^\bullet$	$kP_{O_2}^{1/2}$	$n = 1/2$
2	$(1/2)O_2 + V_O^{\bullet\bullet} \overset{1}{\leftrightarrow} (O \cdots V_O^{\bullet\bullet})$	$k_1 P_{O_2}^{1/2}$	$n = 1/2$
	$(O \cdots V_O^{\bullet\bullet}) \overset{2}{\leftrightarrow} O_O^X + 2h^\bullet$	$K_1^{eq} k_2 P_{O_2}^{1/2}$	$n = 1/2$
3	$(1/2)O_2 \overset{1}{\leftrightarrow} O^*$	$k_1 P_{O_2}^{1/2}\delta_\infty^{-1}$	$1/2 < n = (1/2) + (1/2\Gamma_V) < 1$
	$O^* + V_O^{\bullet\bullet} \overset{2}{\leftrightarrow} O_O^X + 2h^\bullet$	$K_1^{eq} k_2 P_{O_2}^{1/2}$	$n = 1/2$

Mechanism	Reaction mechanism	k_V/L (s^{-1})	k_V order in P_{O_2}
4	$(1/2)O_2 \overset{1}{\leftrightarrow} O^- + h^\bullet$	$k_1 P_{O_2}^{1/2}\delta_\infty^{-1}$	$1/2 < n = (1/2) + (1/2\Gamma_V) < 1$
	$O^- + V_O^{\bullet\bullet} \overset{2}{\leftrightarrow} O_O^X + h^\bullet$	$k_2 K_1^{eq} P_{O_2}^{1/2}(x - 2\delta_\infty)^{-1}$	$1/4 < n = (1/4) + (1/4\Gamma_V) < 1/2$
5	$(1/2)O_2 \overset{1}{\leftrightarrow} O^{-2} + 2h^\bullet$	$k_1 P_{O_2}^{1/2}\delta_\infty^{-1}$	$1/2 < n = (1/2) + (1/2\Gamma_V) < 1$
	$O^{-2} + V_O^{\bullet\bullet} \overset{2}{\leftrightarrow} O_O^X$	$3k_{-2}\delta_\infty^{-1}$	$0 < n = (1/2\Gamma_V) < 1/2$
6	$(1/2)O_2 \overset{1}{\leftrightarrow} O^- + h^\bullet$	$k_1 P_{O_2}^{1/2}\delta_\infty^{-1}$	$1/2 < n = (1/2) + (1/2\Gamma_V) < 1$
	$O^- + V_O^{\bullet\bullet} \overset{2}{\leftrightarrow} O_O^\bullet$	$k_2 K_1^{eq} P_{O_2}^{1/2}(x - 2\delta_\infty)^{-1}$	$1/4 < n = (1/4) + (1/4\Gamma_V) < 1/2$
	$O_O^\bullet \overset{3}{\leftrightarrow} O_O^X + h^\bullet$	$k_{-3} K_{eq} P_{O_2}^{1/2}(x - 2\delta_\infty)^{-1}$	$1/4 < n = (1/4) + (1/4\Gamma_V) < 1/2$
7	$(1/2)O_2 \overset{1}{\leftrightarrow} O^- + h^\bullet$	$k_1 P_{O_2}^{1/2}\delta_\infty^{-1}$	$1/2 < n = (1/2) + (1/2\Gamma_V) < 1$
	$O^- \overset{2}{\leftrightarrow} O^{2-} + h^\bullet$	$k_2 K_1^{eq} P_{O_2}^{1/2}\delta_\infty^{-1}(x - 2\delta_\infty)^{-1}$	$1/4 < n = (1/4) + (3/4\Gamma_V) < 1$
	$O^{2-} + V_O^{\bullet\bullet} \overset{3}{\leftrightarrow} O_O^X$	$3k_{-3}\delta_\infty^{-1}$	$0 < n = (1/2\Gamma_V) < 1/2$
8	$O_2 \overset{1}{\leftrightarrow} O_2^*$	$4k_1 P_{O_2}\delta_\infty^{-1}$	$1 < n = 1 + (1/2\Gamma_V) < 3/2$
	$O_2^* \overset{2}{\leftrightarrow} 2O^*$	$4k_2 K_1^{eq} P_{O_2}\delta_\infty^{-1}$	$1 < n = 1 + (1/2\Gamma_V) < 3/2$
	$O^* + V_O^{\bullet\bullet} \overset{3}{\leftrightarrow} O_O^X + 2h^\bullet$	$k_{-3} K_{eq} P_{O_2}^{1/2}$	$n = 1/2$
9	$O_2 \overset{1}{\leftrightarrow} O_2^- + h^\bullet$	$4k_1 P_{O_2}\delta_\infty^{-1}$	$1 < n = 1 + (1/2\Gamma_V) < 3/2$
	$O_2^- \overset{2}{\leftrightarrow} 2O^- + h^\bullet$	$4k_2 K_1^{eq} P_{O_2}\delta_\infty^{-1}(x - 2\delta_\infty)^{-1}$	$3/4 < n = (3/4) + (3/4\Gamma_V) < 3/2$
	$O^- + V_O^{\bullet\bullet} \overset{3}{\leftrightarrow} O_O^X + h^\bullet$	$k_{-3} K_{eq} P_{O_2}^{1/2}(x - 2\delta_\infty)^{-1}$	$1/4 < n = (1/4) + (1/4\Gamma_V) < 1/2$
10	$O_2 + V_O^{\bullet\bullet} \overset{1}{\leftrightarrow} (O_2 \cdots V_O^{\bullet\bullet})$	$4k_1 P_{O_2}$	$n = 1$
	$(O_2 \cdots V_O^{\bullet\bullet}) + V_O^{\bullet\bullet} \overset{2}{\leftrightarrow} 2(O \cdots V_O^{\bullet\bullet})$	$4k_2 K_1^{eq} P_{O_2}\delta_\infty$	$1/2 < n = 1 - (1/2\Gamma_V) < 1$
	$(O \cdots V_O^{\bullet\bullet}) \overset{3}{\leftrightarrow} O_O^X + 2h^\bullet$	$k_{-3} K_{eq} P_{O_2}^{1/2}$	$n = 1/2$
11	$O_2 + V_O^{\bullet\bullet} \overset{1}{\leftrightarrow} (O_2 \cdots V_O^{\bullet\bullet})$	$4k_1 P_{O_2}$	$n = 1$
	$(O_2 \cdots V_O^{\bullet\bullet}) + V_O^{\bullet\bullet} \overset{2}{\leftrightarrow} (V_O^{\bullet\bullet} \cdots O_2 \cdots V_O^{\bullet\bullet})$	$4k_2 K_1^{eq} P_{O_2}\delta_\infty$	$1/2 < n = 1 - (1/2\Gamma_V) < 1$
	$(V_O^{\bullet\bullet} \cdots O_2 \cdots V_O^{\bullet\bullet}) \overset{3}{\leftrightarrow} 2(O \cdots V_O^{\bullet\bullet})$	$4k_3 K_1^{eq} K_2^{eq} P_{O_2}\delta_\infty$	$1/2 < n = 1 - (1/2\Gamma_V) < 1$
	$(O \cdots V_O^{\bullet\bullet}) \overset{4}{\leftrightarrow} O_O^X + 2h^\bullet$	$k_{-4} K_{eq} P_{O_2}^{1/2}$	$n = 1/2$
12	$O_2 + V_O^{\bullet\bullet} \overset{1}{\leftrightarrow} (O_2 \cdots V_O^{\bullet\bullet})$	$4k_1 P_{O_2}$	$n = 1$
	$(O_2 \cdots V_O^{\bullet\bullet}) + V_O^{\bullet\bullet} \overset{2}{\leftrightarrow} (O \cdots V_O^{\bullet\bullet}) + O^- + h^\bullet$	$4k_2 K_1^{eq} P_{O_2}$	$n = 1$
	$(O \cdots V_O^{\bullet\bullet}) \overset{3}{\leftrightarrow} O_O^X + 2h^\bullet$	$2k_{-3} K_{eq} P_{O_2}^{1/2}$	$n = 1/2$
	$O^- + V_O^{\bullet\bullet} \overset{4}{\leftrightarrow} O_O^X + h^\bullet$	$2k_{-4} K_{eq} P_{O_2}^{1/2}(x - 2\delta_\infty)^{-1}$	$1/4 < n = (1/4) + (1/4\Gamma_V) < 1/2$
13	$O_2 \overset{1}{\leftrightarrow} O_2^- + h^\bullet$	$4k_1 P_{O_2}\delta_\infty^{-1}$	$1 < n = 1 + (1/2\Gamma_V) < 3/2$
	$O_2^- \overset{2}{\leftrightarrow} O_2^{2-} + h^\bullet$	$4k_2 K_1^{eq} P_{O_2}\delta_\infty^{-1}(x - 2\delta_\infty)^{-1}$	$3/4 < n = (3/4) + (3/4\Gamma_V) < 3/2$
	$O_2^{2-} \overset{3}{\leftrightarrow} 2O^-$	$12k_3 K_1^{eq} K_2^{eq} K_{eq}^{-1} P_{O_2}^{1/2}\delta_\infty^{-2}$	$1/2 < n = (1/2) + (1/\Gamma_V) < 3/2$
	$O^- + V_O^{\bullet\bullet} \overset{4}{\leftrightarrow} O_O^X + h^\bullet$	$k_{-4} K_{eq} P_{O_2}^{1/2}(x - 2\delta_\infty)^{-1}$	$1/4 < n = (1/4) + (1/4\Gamma_V) < 1/2$

Mechanism	Reaction mechanism	k_V/L (s⁻¹)	k_V order in P_{O_2}
14	$O_2 \overset{1}{\leftrightarrow} O_2^*$ $O_2^* \overset{2}{\leftrightarrow} 2O^*$ $O^* \overset{3}{\leftrightarrow} O^- + h^\bullet$ $O^- + V_O^{\bullet\bullet} \overset{4}{\leftrightarrow} O_O^X + h^\bullet$	$4k_1 P_{O_2}\delta_\infty^{-1}$ $4k_2 K_1^{eq} P_{O_2}\delta_\infty^{-1}$ $k_3\sqrt{K_1^{eq}K_2^{eq}}P_{O_2}^{1/2}\delta_\infty^{-1}$ $k_{-4}K_{eq}(x-2\delta_\infty)^{-1}$	$1 < n = 1 + (1/2\Gamma_V) < 3/2$ $1 < n = 1 + (1/2\Gamma_V) < 3/2$ $1/2 < n = (1/2) + (1/2\Gamma_V) < 1$ $-1/4 < n = -[(1/4) - (1/4\Gamma_V)] < 0$
15	$O_2 \overset{1}{\leftrightarrow} O_2^*$ $O_2^* \overset{2}{\leftrightarrow} 2O^*$ $O^* \overset{3}{\leftrightarrow} O^- + h^\bullet$ $O^- \overset{4}{\leftrightarrow} O^{2-} + h^\bullet$ $O^{2-} + V_O^{\bullet\bullet} \overset{5}{\leftrightarrow} O_O^X$	$4k_1 P_{O_2}\delta_\infty^{-1}$ $4k_2 K_1^{eq} P_{O_2}\delta_\infty^{-1}$ $k_3\sqrt{K_1^{eq}K_2^{eq}}P_{O_2}^{1/2}\delta_\infty^{-1}$ $k_4\sqrt{K_1^{eq}K_2^{eq}}P_{O_2}^{1/2}\delta_\infty^{-1}(x-2\delta_\infty)^{-1}$ $3k_{-5}\delta_\infty^{-1}$	$1 < n = 1 + (1/2\Gamma_V) < 3/2$ $1 < n = 1 + (1/2\Gamma_V) < 3/2$ $1/2 < n = (1/2) + (1/2\Gamma_V) < 1$ $1/4 < n = (1/4) + (3/4\Gamma_V) < 1$ $0 < n = (1/2\Gamma_V) < 1/2$
16	$1/2 O_2 \overset{1}{\leftrightarrow} O^*$ $O^* \overset{2}{\leftrightarrow} O^{2-} + 2h^\bullet$ $O^{2-} + V_O^{\bullet\bullet} \overset{3}{\leftrightarrow} O_O^X$	$k_1 P_{O_2}^{1/2}\delta_\infty^{-1}$ $k_2 K_1^{eq} P_{O_2}^{1/2}\delta_\infty^{-1}$ $3k_{-3}\delta_\infty^{-1}$	$1/2 < n = (1/2) + (1/2\Gamma_V) < 1$ $1/2 < n = (1/2) + (1/2\Gamma_V) < 1$ $0 < n = (1/2\Gamma_V) < 1/2$
17	$O_2 \overset{1}{\leftrightarrow} O_{ads} + O^{-2}$ $O_{ads} \overset{2}{\leftrightarrow} O^{-2} + 2h^\bullet$ $O^{-2} + V_O^{\bullet\bullet} \overset{3}{\leftrightarrow} O_O^X$	$4k_1 P_{O_2}\delta_\infty^{-1}$ $2k_{-2}\sqrt{K_1^{eq}K_2^{eq}}P_{O_2}^{1/2}\delta_\infty^{-1}$ $3k_{-3}\delta_\infty^{-1}$	$1 < n = 1 + (1/2\Gamma_V) < 3/2$ $1/2 < n = (1/2) + (1/2\Gamma_V) < 1$ $0 < n = (1/2\Gamma_V) < 1/2$
18	$O_2 + V_O^{\bullet\bullet} \overset{1}{\leftrightarrow} (O_2 \cdots V_O^{\bullet\bullet})$ $(O_2 \cdots V_O^{\bullet\bullet}) + V_O^{\bullet\bullet} \overset{2}{\leftrightarrow} 2O_O^X + 4h^\bullet$	$4k_1 P_{O_2}$ $4k_2 K_1^{eq} P_{O_2}\delta_\infty$	$n = 1$ $1/2 < n = 1 - (1/2\Gamma_V) < 1$
19	$O_2 + (V_O^{\bullet\bullet} \cdots V_O^{\bullet\bullet}) \overset{1}{\leftrightarrow} 2(O \cdots V_O^{\bullet\bullet})$ $(O \cdots V_O^{\bullet\bullet}) \overset{2}{\leftrightarrow} O_O^X + 2h^\bullet$	$4k_1 P_{O_2}\delta_\infty$ $k_{-2}K_{eq}P_{O_2}^{1/2}$	$1/2 < n = 1 - (1/2\Gamma_V) < 1$ $n = 1/2$
20	$O_2 \overset{1}{\leftrightarrow} O_2^{2-} + 2h^\bullet$ $O_2^{2-} \overset{2}{\leftrightarrow} 2O^-$ $O^- + V_O^{\bullet\bullet} \overset{3}{\leftrightarrow} O_O^X + h^\bullet$	$4k_1 P_{O_2}\delta_\infty^{-1}$ $12k_2 K_1^{eq}K_{eq}^{-1}P_{O_2}^{1/2}\delta_\infty^{-2}$ $k_{-3}K_{eq}P_{O_2}^{1/2}\delta_\infty^{-1}(x-2\delta_\infty)^{-1}$	$1 < n = 1 + (1/2\Gamma_V) < 3/2$ $1/2 < n = (1/2) + (1/\Gamma_V) < 3/2$ $1/4 < n = (1/4) + (3/4\Gamma_V) < 1$
21	$O_2 \overset{1}{\leftrightarrow} O_2^*$ $O_2^* \overset{2}{\leftrightarrow} O_2^- + h^\bullet$ $O_2^- \overset{3}{\leftrightarrow} O_2^{2-} + h^\bullet$ $O_2^{2-} \overset{4}{\leftrightarrow} 2O^-$ $O^- + V_O^{\bullet\bullet} \overset{5}{\leftrightarrow} O_O^X + h^\bullet$	$4k_1 P_{O_2}\delta_\infty^{-1}$ $4k_2 K_1^{eq}P_{O_2}\delta_\infty^{-1}$ $k_3 K_1^{eq}K_2^{eq}P_{O_2}\delta_\infty^{-1}(x-2\delta_\infty)^{-1}$ $12k_{-4}K_{eq}(K_5^{eq})^{-2}P_{O_2}^{1/2}\delta_\infty^{-2}$ $k_{-5}K_{eq}P_{O_2}^{1/2}$	$1 < n = 1 + (1/2\Gamma_V) < 3/2$ $1 < n = 1 + (1/2\Gamma_V) < 3/2$ $3/4 < n = (3/4) + (3/4\Gamma_V) < 3/2$ $1/2 < n = (1/2) + (1/\Gamma_V) < 3/2$ $n = 1/2$
22	$O_2 + V_O^{\bullet\bullet} \overset{1}{\leftrightarrow} (O_2 \cdots V_O^{\bullet\bullet})$ $(O_2 \cdots V_O^{\bullet\bullet}) + * \overset{2}{\leftrightarrow} O_O^X + 2h^\bullet + O^*$ $O^* + V_O^{\bullet\bullet} \overset{3}{\leftrightarrow} O_O^X + 2h^\bullet + *$	$\dfrac{k_V}{L} = \dfrac{4k_{-3}K_{eq}P_{O_2}}{k_- + P_{O_2}^{1/2}}$ $k_- = \dfrac{k_3}{K_{eq}}\left(\dfrac{1}{k_{-2}} + \dfrac{K_2^{eq}}{k_{-1}}\right)$	$n = 1$ $n = 1$ $n = 1/2$

1. $\delta_\infty \propto P_{O_2}^{-1/2\Gamma_V}$, $(x-2\delta_\infty) \propto P_{O_2}^{(1/4)-(1/4\Gamma_V)}$, $\Gamma_V \gtrsim 1$

References

1. J. E. tenElshof, H. J. M. Bouwmeester, and H. Verweij, *Solid State Ionics*, **81**, 97 (1995).
2. H. J. M. Bouwmeester, H. Kruidhof, and A. J. Burggraaf, *Solid State Ionics*, **72**, 185 (1994).
3. T. Ishigaki, S. Yamauchi, K. Kishio, J. Mizusaki, and K. Fueki, *J. Solid State Chem.*, **73**, 179 (1988).
4. M. V. Patrakeev, J. A. Bahteeva, E. B. Mitberg, I. A. Leonidova, V. L. Kozhevni-

kov, and K. R. Poeppelmeier, *J. Solid State Chem.*, **172**, 219 (2003).

5. M. V. Patrakeev, I. A. Leonidov, V. L. Kozhevnikov, and K. R. Poeppelmeier, *J. Solid State Chem.*, **178**, 921 (2005).

6. J. A. Bahteeva, I. A. Leonidov, M. V. Patrakeev, E. B. Mitberg, V. L. Kozhevnikov, and K. R. Poeppelmeier, *J. Solid State Electrochem.*, **8**, 578 (2004).

7. E. V. Bongio, H. Black, F. C. Raszewski, D. Edwards, C. J. McConville, and V. R. W. Amarakoon, *J. Electroceram.*, **14**, 193 (2005).

8. M. C. Kim, S. J. Park, H. Haneda, J. Tanaka, and S. Shirasaki, *Solid State Ionics*, **40-1**, 239 (1990).

9. J. Mizusaki, T. Sasamoto, W. R. Cannon, and H. K. Bowen, *J. Am. Ceram. Soc.*, **66**, 247 (1983).

10. J. Mizusaki, M. Yoshihiro, S. Yamauchi, and K. Fueki, *J. Solid State Chem.*, **58**, 257 (1985).

11. J. Mizusaki, M. Yoshihiro, S. Yamauchi, and K. Fueki, *J. Solid State Chem.*, **67**, 1 (1987).

12. M. Søgaard, P. V. Hendriksen, and M. Mogensen, *J. Solid State Chem.*, **180**, 1489 (2007).

13. M. Søgaard, Ph.D. Thesis, Risø National Laboratory (2005).

14. J. E. tenElshof, M. H. R. Lankhorst, and H. J. M. Bouwmeester, *J. Electrochem. Soc.*, **144**, 1060 (1997).

15. J. Yoo, A. Verma, S. Y. Wang, and A. J. Jacobson, *J. Electrochem. Soc.*, **152**, A497 (2005).

16. I. Yasuda and T. Hikita, *J. Electrochem. Soc.*, **141**, 1268 (1994).

17. C. R. Song and H. I. Yoo, *Solid State Ionics*, **124**, 289 (1999).

18. M. Søgaard, P. V. Hendriksen, M. Mogensen, F. W. Poulsen, and E. Skou, *Solid State Ionics*, **177**, 3285 (2006).

19. S. Kim, S. Wang, X. Chen, Y. L. Yang, N. Wu, A. Ignatiev, A. J. Jacobson, and B. Abeles, *J. Electrochem. Soc.*, **147**, 2398 (2000).

20. J. Maier, *Solid State Ionics*, **112**, 197 (1998).

21. J. Maier, *Solid State Ionics*, **135**, 575 (2000).

22. S. B. Adler, X. Y. Chen, and J. R. Wilson, *J. Catal.*, **245**, 91 (2007).

23. P. J. Gellings and H. J. M. Bouwmeester, *Catal. Today*, **58**, 1 (2000).

24. R. Merkle and J. Maier, *Phys. Chem. Chem. Phys.*, **4**, 4140 (2002).

25. R. Merkle, J. Maier, and H. J. M. Bouwmeester, *Angew. Chem., Int. Ed.*, **43**, 5069 (2004).

26. R. Merkle and J. Maier, *Top. Catal.*, **38**, 141 (2006).

27. J. Deseure, Y. Bultel, L. Dessemond, and E. Siebert, *Solid State Ionics*, **176**, 235 (2005).

28. K. J. Laidler, *Chemical Kinetics*, Harper & Row, New York (1987).

29. M. Mosleh, N. Pryds, and P. V. Hendriksen, *Mater. Sci. Eng., B*, **144**, 38 (2007).

30. K. Sasaki and J. Maier, *Solid State Ionics*, **161**, 145 (2003).

31. X. Chen, S. Wang, Y. L. Yang, L. Smith, N. J. Wu, B. I. Kim, S. S. Perry, A. J. Jacobson, and A. Ignatiev, *Solid State Ionics*, **146**, 405 (2002).

32. R. Ganeshananthan and A. V. Virkar, *J. Electrochem. Soc.*, **152**, A1620 (2005).

33. M. Mogensen, K. V. Hansen, in *Handbook of Fuel Cells*, Vol. 5, W. Vielstich, H. A. Gasteiger, and H. Yokokawa, Editors, John Wiley & Sons, Hoboken, NJ (2008).

34. W. Preis, E. Bucher, and W. Sitte, *Solid State Ionics*, **175**, 393 (2004).

35. J. Nowotny, in *The CRC Handbook of Solid State Electrochemistry*, P. J. Gellings and H. J. M. Bouwmeester, Editors, CRC Press, Boca Raton, (1997).

36. H. J. M. Bouwmeester, and A. J. Burggraaf, in *The CRC Handbook of Solid State Electrochemistry*, P. J. Gellings and H. J. M. Bouwmeester, Editors, CRC Press, Boca Raton (1997).

37. M. W. den Otter, H. J. M. Bouwmeester, B. A. Boukamp, and H. Verweij, *J. Electrochem. Soc.*, **148**, J1 (2001).

38. Z. P. Shao, G. X. Xiong, H. Dong, W. H. Yang, and L. W. Lin, *Appl. Spectrosc.*, **25**, 97 (2001).

39. J. A. Kilner, R. A. DeSouza, and I. C. Fullarton, *Solid State Ionics*, **86-8**, 703 (1996).

40. R. A. DeSouza and J. A. Kilner, *Solid State Ionics*, **126**, 153 (1999).